High density lipoproteins improve insulin sensitivity in high fat diet fed mice by suppressing hepatic inflammation

Kristine C. McGrath[1,2], Xiao Hong Li[2,5], Phillippa T. Whitworth[1], Robert Kasz[1], Joanne T. Tan[2], Susan V. McLennan[3], David S. Celermajer[2,3,4], Philip J. Barter[2,6], Kerry-Anne Rye[2,6], Alison K. Heather[1,2]

1. University of Technology, Sydney, School of Medical and Molecular Biosciences, Faculty of Science, Broadway, NSW, Australia
2. The Heart Research Institute, Newtown, NSW, Australia
3. University of Sydney, Discipline of Medicine, Sydney, NSW, Australia
4. Royal Prince Alfred Hospital, Department of Cardiology, Camperdown, NSW, Australia
5. Dezhou people's Hospital, Department of Endocrinology, Shandong, China
6. University of New South Wales, Faculty of Medicine, Randwick, NSW, Australia

Abbreviated Title: *HDLs improves insulin sensitivity*

Corresponding Author

Professor Alison Heather

University of Technology, Sydney

PO Box 123, Broadway

Ultimo, NSW, 2007, Australia

Ph. 612 9514 4034

Fax: 612 9514 8206

Email: alison.heather@uts.edu.au

ABBREVIATIONS: AMP-activated protein kinase, AMPK; Carbohydrate responsive element–binding protein, ChREBP; Glucose-6-phosphatase, G6Pase; Homeostatic model assessment of insulin resistance, HOMA-IR; Human hepatoma cell line, HuH-7; Inhibitor kappa B, IκB; Inhibitor of nuclear factor kappa-B kinase subunit beta, IKK-β; Interleukin 1 beta, IL-1β; Interleukin 6, IL-6; Intraperitoneal glucose tolerance test, IPGTT; Intraperitoneal insulin tolerance test, IPITT; Nuclear factor kappa B, NF-κB; 1-palmitoyl-2-linoleoyl-sn-glycero-3-phosphatidylcholine, PLPC; Reconstituted apolipoprotein AI HDL, rHDLs; Serum amyloid A1, SAA1; Standard chow diet, StD; Sterol regulatory element binding protein 1, SREBP-1; Tumor necrosis factor alpha, TNF-α.

ABSTRACT

Obesity-induced liver inflammation can drive insulin resistance. HDL has anti-inflammatory properties so we hypothesized that low levels of HDL perpetuate inflammatory responses in the liver and that HDL treatment will suppress liver inflammation and insulin resistance. The aim of this study was to investigate the effects of lipid-free apoAI on hepatic inflammation and insulin resistance in mice. We also investigated apoAI as a component of reconstituted HDL (rHDLs) in hepatocytes to confirm results we observe *in vivo*. To test our hypothesis, C57BL/6 mice were fed a high-fat diet (HFD) for 16-weeks and administered either saline or lipid-free apoAI. Injections of lipid-free apoAI twice a week for 2- or 4- weeks with lipid-free apoAI resulted in: (i) improved insulin sensitivity associated with decreased systemic and hepatic inflammation; (ii) suppression of hepatic mRNA expression for key transcriptional regulators of lipogenic gene expression and; (iii) suppression of NF-κB activation. Human hepatoma HuH-7 cells exposed to rHDLs showed suppressed TNF-α-induced NF-κB activation, correlating with decreased NF-κB target gene expression. We conclude that apoAI suppressed liver inflammation in HFD mice and improved insulin resistance via a mechanism that involves a downregulation of NF-κB activation.

Supplementary key words: High-fat diet, insulin resistance, high density lipoproteins, apolipoprotein AI, inflammation, cellular signalling.

INTRODUCTION

Hepatic inflammation can induce insulin resistance via an imbalance in the secretion of pro-inflammatory cytokines, subsequent to activation of inflammatory/oxidative transcription factors (1). A key transcription factor that mediates the inflammatory response in hepatocytes is nuclear factor-κB (NF-κB) (2, 3). Activated hepatic NF-κB alone can drive insulin resistance as evidenced by the finding that transgenic expression of IκB kinase, IKK-β, which increases NF-κB activity, results in overt insulin resistance in mice fed a normal chow diet (4). Conversely, when heterozygous IKK-$\beta^{+/-}$ mice expressing low levels of NF-κB are fed a high-fat diet, or are crossed with *ob/ob* mice, they do not develop insulin resistance (5). Moreover, genetic manipulation to inhibit hepatic NF-κB activity directly protects against insulin resistance in response to a high-fat diet in mice (4). Such findings provide strong evidence that the liver is a primary site of inflammatory action that causes insulin resistance and that NF-κB is a central pathogenic factor underlying inflammation-induced insulin resistance.

NF-κB activation increases the secretion of a number of pro-inflammatory cytokines, including IL-6, TNF-α and IL-1β (1). NF-κB activation involves a complex series of signalling events that begins with activation of the IκB kinase complex that, in turn, phosphorylates inhibitor κB (IκB) (6, 7). IκB is an inhibitor protein of NF-κB that binds to NF-κB, sequestering it in the cytoplasm (8). However, once phosphorylated, IκB is targeted for ubiquitination and subsequent degradation, leaving NF-κB free to translocate to the nucleus and initiate transcription of target genes (9).

High density lipoproteins (HDLs) have potent anti-inflammatory effects (10, 11). We have previously reported that pre-treatment of human coronary artery endothelial cells (HCAEC) with HDLs inhibits TNFα-induced NF-κB activation (12). In addition, injections

of human apolipoprotein A-I (apoAI) (the major HDL protein) into rabbits inhibits vascular inflammation (10). HDL levels are reportedly low in subjects with insulin resistance (13) so this led us to question whether raising HDL may improve insulin resistance by targeting the heightened hepatic inflammatory state. We show that injections of lipid-free apoAI decrease both hepatic and systemic cytokine levels, suppress hepatic NF-κB activation and improve insulin sensitivity in high-fat fed C57BL/6 mice. Moreover, we demonstrate that apoAI-containing reconstituted HDLs (rHDLs) mediate their anti-inflammatory effects in cultured hepatocytes via suppression of the IKK/IκB/NF-κB signalling pathway.

MATERIALS AND METHODS

Preparation of lipid-free apolipoprotein A-I (apoAI) and discoidal reconstituted HDLs (rHDLs)

HDLs were isolated from pooled human plasma (Gribbles Pathology, Adelaide, SA, Australia) by sequential ultracentrifugation in the 1.063-1.21 g/ml density range. Lipid-free apoAI was then isolated from HDL as previously described (14). Discoidal rHDLs containing apoAI complexed to 1-palmitoyl-2-linoleoyl-sn-glycero-3-phosphatidylcholine (PLPC; Avanti Polar Lipids, Alabaster, Alabama, USA) were prepared by the cholate dialysis method (15). The PLPC:apoAI molar ratio was 100:1. Immediately before use in experiments, lipid-free apoAI or rHDLs preparations were dialysed extensively against endotoxin-free phosphate buffered saline (PBS; Sigma-Aldrich, Castle Hill, NSW, Australia)(pH 7.4).

Animal Model

Five week old C57BL/6 male mice purchased from Monash Animal Services (Monash University, VIC, Australia) were housed at the Heart Research Institute Biological Services facility (Sydney, NSW, Australia) and kept at a temperature of 21°C ± 2°C on a 12:12 h light/dark cycle. All experiments were approved by the South Western Sydney Area Health Service Animal Welfare Committee. At 6 weeks of age, the mice were randomised into four groups: (1) Control mice (n=10) were fed a standard chow diet (StD:14.3 MJ/kg; 65% of energy from carbohydrate (wheat, barley, lupins); 12% from fat (mixed vegetable oils, canola oil); 23% from protein (soya meal, fish meal); Specialty Feeds, Glen Forrest, WA, Australia); (2) Mice (n=10) fed a high-fat diet (HFD: 19.4 MJ/kg; 43% of energy from carbohydrate – sucrose, cellulose, wheat starch; 40% from fat-clarified butter (Ghee), cholesterol, 17% from protein (casein); SF00-219, Specialty Feeds) ad libitum for 16 weeks total. At 18 weeks of age and 13 weeks of HFD this subset of mice received endotoxin-free

PBS (vehicle control) by tail vein injection twice weekly for the last 4 weeks of the diet; (3) Mice (n=10) fed a HFD ad libitum for 16 weeks total. At 18 weeks of age and 13 weeks of HFD this subset of mice received apoAI by tail vein injection twice weekly for the last 4 weeks of the diet and; (4) Mice (n=10) fed a HFD ad libitum for 16 weeks total. At 20 weeks of age and 15 weeks of HFD this subset of mice received apoAI by tail vein injection twice weekly for the last 2 weeks of the diet. ApoA-I was administered at a dose of 8 mg/kg. Animals were sacrificed at 24 hours after their final injection by right atrium exsanguination after methoxyflurane (Medical Developments International, Springvale, VIC, Australia) anaesthesia. Blood samples were centrifuged (1,000 x *g* for 10 min) and the subsequent serum fraction collected and stored at –20°C. Liver tissue was rapidly excised, snap frozen in liquid nitrogen and stored at –80°C.

Glucose-, insulin tolerance and pyruvate challenge tests, fasting serum triglyceride, cytokine and insulin measurements.

At the end of the study, an intraperitoneal glucose tolerance test (IPGTT), an intraperitoneal insulin tolerance test (IPITT) and a pyruvate challenge test were performed in overnight fasted mice. Blood samples were obtained from the tail tip at the indicated times and glucose levels were measured using a glucometer (Accu-Chek, Roche, Castle Hill, NSW, Australia). The doses used during these tests were glucose at 1 g/kg body weight, insulin at 0.75 IU/kg body weight and pyruvate at 2 g/kg body weight for IPGTT, IPITT and pyruvate challenge test, respectively. Serum triglyceride levels were measured with triglyceride reagent (Roche Diagnostics, Castle Hill, NSW, Australia). Serum cytokine levels were determined using a mouse Bioplex Kit (Bio-Rad, Hercules, CA, USA). Insulin levels were measured using an enzyme-linked immunosorbent assay (Crystal Chem, Downers Grove, IL,

USA). The homeostatic model assessment of insulin resistance (HOMA-IR) was determined for each mouse (4).

Intrahepatic neutral lipid accumulation assay

The level of neutral lipids (triglyceride plus cholesterol esters) accumulated in the liver was determined by measurement of Oil Red-O of tissue extracts by quantitative assay (16). Briefly, frozen liver tissue (100 mg) was homogenized and incubated with an Oil Red-O solution (0.15% Oil Red-O, 0.4% dextrin) for 60 min. The samples were washed with 60% isopropanol to remove excess dye and the dye incorporated into lipid was then extracted with 99% isopropanol and quantified by measurement of absorbance at 520 nm (16).

Cell culture

A human hepatoma cell line (HuH-7; Health Science Research Resources Bank, Osaka, Japan) were cultured in DMEM/F12 medium (Sigma-Aldrich) with 10% FBS at 37°C in 5% CO_2. Unless otherwise stated, HuH-7 cells were pre-incubated for 16 hours with rHDLs (final apoAI concentration, 16 μmol/l or 0.45 mg/ml), PBS (control), sodium salicylate (5 mmol/l, Sigma-Aldrich) or the IKK inhibitor, Wedelolactone (8 mmol/l, Calbiochem, Gibbstown, NJ, USA) then stimulated with TNF-α (1 ng/mL) for 24 hours. For some cells, after the 16-hour incubation, the rHDL-containing medium was removed and cells were washed twice with PBS before fresh medium supplemented with TNF-α (1 ng/mL) was added for 24 hours. Non-TNF-α-stimulated, PBS treated cells acted as controls.

Cholesterol depletion and repletion

Cholesterol depletion was performed by incubating HuH-7 cells with 1.5% methyl-*β*-cyclodextrin for 1 hour at 37°C. To perform cholesterol repletion, cholesterol (0.4

mg/ml) was mixed by vortexing with methyl-β-cyclodextrin (10%) at a 1:20 ratio at 40°C. Following incubation of HuH-7 cells with rHDL for 16 hour, cholesterol repletion was performed by the addition of the cholesterol/cyclodextrin solution diluted at 1:25 for another hour.

Lactate dehydrogenase (LDH) cell viability assay

HuH-7 cells were incubated for 40 hours with rHDLs (final apoAI concentration, 16 µmol/l or 0.45 mg/ml), PBS (control) or sodium salicylate (5 mmol/l, Sigma-Aldrich). Following incubation, cell media was collected and stored on ice. The cells were then washed with PBS and lysed in 1 mL of water for 20 min at 4°C. After centrifugation (1000 x *g*, 5 min) to pellet and remove cell debris, 10 µL cell lysate or cell media were incubated with 200 µL of 0.15 mg/mL NADH and 2.5 mmol/l sodium pyruvate PBS working reagent. The absorbance at 340 nm was determined at 5 min intervals for 35 min (Tecan Sunrise; Tecan Group Ltd, Mannedorf, Switzerland). Viability was calculated from the relative activity of LDH measured for the media versus total activity (17).

Transient cell transfections and luciferase measurements

HuH-7 cells were transfected with an NF-κB-luciferase reporter vector (Promega Corporation, Madison, WI, USA) together with a transfection control plasmid, pRL-TK (Promega) using Effectene (Qiagen, Hilden, Germany) (18). Transfected cells were pre-incubated with rHDLs (final apoAI concentration, 16 µmol/l or 0.45 mg/ml) then stimulated with 1 ng/mL TNF-α (rHDL+TNFα). A subset of transfected cells were pre-incubated with rHDLs but the rHDLs were removed from the culture media prior to activation with TNF-α (rHDL//TNFα). After treatment, cells were washed with PBS and then lysed with passive lysis buffer (Promega). Samples were collected, centrifuged to remove cell debris and then

assayed for luciferase and renilla activity using the Dual-Luciferase Reporter System (Promega). Measurements were obtained using the Fluoroskan Ascent FL luminometer (Thermo Labsystems, Waltham, MA, USA).

IκB kinase (IKK) assay

HuH-7 cells were pre-treated with rHDLs (final apoAI concentration, 16 μmol/l or 0.45 mg/ml) or PBS, then stimulated with TNF-α (1 ng/ml) for 15 min. The cells were lysed in RIPA lysis buffer containing 1% Nonidet P-40, 0.1% SDS, 0.5% deoxycholate, 150 mmol/l NaCl, 50 mmol/l Tris, pH 8 and a protease inhibitor cocktail (Sigma-Aldrich). The protein lysate (10 μg) was incubated with 2 mmol/l ATP and 10 μg IKK substrate peptide (Millipore, Billerica, MA, USA) in reaction buffer (8 mmol/l MOPS, pH 7, 0.2 mmol/l EDTA-Na_2) at room temperature for 90 min. Kinase-Glo reagent (50 μl; Promega) was then added to the reaction mixture, incubated at room temperature for 10 min and the luminescent signal was measured on a Fluoroskan Ascent FL (Thermo Labsystems).

IκB Assay

Whole cell protein lysate was extracted from HuH-7 cells in RIPA lysis buffer as described for the IKK assay. The protein lysate (100 mg) was assayed for IκB-α levels using the PathScan Phospho-IκBα and Total IκBα enzyme-linked immunosorbent assay (Cell Signaling Technology, Danvers, MA, USA).

NF-κB nuclear translocation assay

Nuclear proteins were extracted from HuH-7 cells or liver samples using the NucBuster protein extraction kit (Merck & Co., Whitehouse Station, NJ, USA). Nuclear

proteins (100 μg) were assayed using the NF-κB NoShift transcription factor assay kit (Merck & Co.).

Human NF-κB Target Gene Array Analysis

Total RNA was isolated from HuH-7 cells using TRI reagent (Sigma-Aldrich). Biotin-labelled cDNA probes were prepared from 10 μg of total RNA using AMV reverse transcriptase (Promega) and biotin dUTP. The cDNA probes were then hybridized to the TranSignal NF-κB Target Gene array (Panomics, Santa Clara, CA, USA). Direct chemiluminescence imaging was performed using the ChemiDoc XRS (Bio-Rad, Hercules, CA, USA) imaging system. Quantity One software (Bio-Rad) was used for pairwise comparative gene expression after signal intensities were converted to a ratio adjusted for background and reference gene expression. The array reproducibility was verified by RT-qPCR for genes of interest.

Isolation of total mRNA and analysis by RT-qPCR

Total RNA was extracted from HuH-7 cells or liver samples using TRI reagent (Sigma-Aldrich) and the concentration normalized to 100 ng/μL using the SYBR Green II assay (Molecular Probes, Invitrogen, Melbourne, Australia). RNA integrity was determined with the Experion system (Bio-Rad). cDNA was reverse transcribed from total RNA (100 ng) using iSCRIPT (Bio-Rad). Gene expression (see ESM Table I for primer sequences) was amplified by PCR in reaction mixtures containing 12 pmol primers and iQ SYBR Green Supermix. Amplification was performed in a Bio-Rad iQ5 thermocycler using the following protocol: 95°C for 30 sec, 60°C for 30 sec and 72°C for 30 sec. Relative change in mRNA gene expression was determined by the ΔΔCT approach (19), using *β-2-microglobulin* (*β2M*)

levels as the reference gene for human samples or *transcription factor IID* (*Tbp*) for mouse samples.

Statistical Analysis

Data are expressed as mean±SEM. Significant differences in treatments were determined by one-way ANOVA with Bonferroni's post-test analysis. PRISM software was used for analysis. Significance was set at a two tailed *p*-value <0.05.

RESULTS

ApoAI improves glucose tolerance, insulin sensitivity and hepatic glucose metabolism in HFD-fed mice

HFD-fed C57BL/6 mice had a 14-15 g (p<0.05) increase in body weight compared to StD-fed mice over the 16-week study period (Fig. 1A). The increase in body weight was associated with increased serum triglyceride, hepatic neutral lipid (triglyceride plus cholesterol esters) levels (ESM Fig. IIIA,B p<0.01 for both) and key transcriptional regulators of lipogenic gene expression in the liver sterol regulatory element binding protein 1 (SREBP-1) and carbohydrate responsive element–binding protein (ChREBP)(p<0.001; Fig. 1B,C). The HFD-induced increase in body weight was not affected by the apoAI treatments, however suppressed the HFD-induced increase in serum triglyceride, hepatic neutral lipid (triglyceride plus cholesterol esters) levels, *SREBP-1* and *ChREBP* levels (ESM Fig. IIIA, B and Fig. 1B, C, respectively).

Insulin resistance as measured by the homeostasis model assessment-IR (HOMA-IR, (1)) was 12-fold higher in the HFD-fed C57BL/6 mice than in the control animals (ESM Fig. I). Both 2 and 4 weeks of treatment with apoAI reduced the HOMA-IR in the HFD-fed animals by 2.81±0.97-fold and 2.85±0.4-fold, respectively (p<0.05 for both). HFD-fed mice displayed glucose intolerance, with levels of both fasting insulin (ESM Fig. IIA, p<0.05) and glucose (ESM Fig. IIB, p<0.05) being increased by 3.2±0.5-fold and 1.44±0.7-fold, respectively. Treatment with apoAI for 2 and 4 weeks significantly reduced fasting insulin and glucose levels. These results were consistent with the apoAI treatment improving IPGTT and IPITT (Fig. 2A-D). ApoAI treatment also improved hepatic glucose metabolism as determined by the pyruvate challenge assay (Fig. 2E,F). This was associated with an apoAI-induced suppression of mRNA levels encoding the rate-limiting enzymes in gluconeogenesis,

phosphoenolpyruvate carboxykinase (PEPCK) and glucose-6-phosphatase (G6Pase) (Table 1).

Cytokine expression following ApoAI-treatments

Serum cytokine levels were measured to assess systemic inflammation. HFD-fed mice had elevated serum concentrations of TNF-α ($p<0.05$), IL-6 ($p<0.001$) and IFN-γ ($p< 0.001$), compared to StD-fed mice (Fig. 3). ApoAI treatment for both 2 and 4 weeks reduced serum levels of IL-6 by 94±0.13% ($p<0.01$) and 96±9% ($p<0.01$), respectively. Similarly, the apoAI-treatments significantly reduced serum levels of IFN-γ and TNF-α by 36-58±9-19% ($p<0.05$).

Table 1 shows that treatment with apoAI significantly decreased TNF-α, IL-6, IFN-γ, IL-1β and SAA1 hepatic mRNA levels in the HFD mice. Mice consuming the HFD had an increased number of macrophages (Kupffer cells) in the liver as demonstrated by an increase in mRNA levels of the macrophage-specific genes *CD68* and *F4/80*. Treatment of the HFD mice with apoAI for 2 or 4 weeks decreased the hepatic expression of both *CD68* and *F4/80* (Table 1).

ApoAI- suppressed activated NF-κB levels

NF-κB is the key regulator of *TNF-α, IL-6, IFN-γ, IL-1β* and *SAA1* gene expression in the liver (20, 21). As shown in Fig. 4, the HFD-fed mice had a 30±3% ($p<0.05$) increase in hepatic nuclear NF-κB levels relative to levels in the StD-fed mice. Treatment with apoAI decreased NF-κB levels and, in the animals treated with apoAI for 4 weeks, the NF-κB nuclear levels were returned to those observed in the StD-fed mice.

We have previously shown that apoAI as a component of discoidal rHDLs suppressed NF-κB activation through increased expression of DHCR24, and that this enzyme is at least, in part, responsible for mediating the anti-inflammatory effects of rHDLs in human coronary aortic endothelial cells (12). ESM Fig. IV shows there was no change in hepatic DHCR24 mRNA expression in HFD-fed mice treated with apoAI for 2 or 4 weeks.

rHDLs suppressed classical NF-κB signalling in cultured human hepatocytes

The human transformed liver cell line (HuH-7) was transfected with an NF-κB-luciferase reporter vector, then pre-incubated for 16 hours with discoidal rHDLs (final apoAI concentration, 16 μmol/l or 0.45 mg/ml). After exposure to rHDLs, the HuH-7 cells were stimulated with TNF-α for 5 hours to induce inflammation. Cells pre-treated with PBS alone before being activated with TNF-α acted as positive controls. Fig. 5A shows that exposure to TNF-α increased NF-κB activation by 80±8% *(p*<0.0001), an effect that was abrogated in the cells pre-treated with rHDLs (rHDL+TNFα). The effect of rHDLs was not due to blockade of the TNF-α receptor as the effects of the rHDLs was sustained even if the rHDLs were removed from the culture media prior to TNF-α stimulation (rHDL//TNFα). Using an NF-κB nuclear translocation assay, Fig. 5B confirms the reporter assay results with pre-treatment with rHDLs decreasing TNF-α-induced nuclear NF-κB levels.

We next examined whether rHDLs (final apoAI concentration, 16 μmol/l or 0.45 mg/ml) treatment decreased IKK activation thereby stopping IκBα degradation. As shown TNF-α increased IKK activity by 16±0.7% (*p*<0.01; Fig. 5C), this effect was abrogated by rHDL treatment *(p*<0.05). Treatment with the rHDLs also effectively blocked IκBα phosphorylation as measured by an ELISA for phosphorylated-IκBα versus total IκBα (Fig. 5D).

rHDL anti-inflammatory effects are not via cholesterol mobilization

The anti-inflammatory effects of rHDL may be due to rHDL-mediated cholesterol mobilization from the plasma membrane. Figure 6 shows cholesterol depletion by treatment with 1.5% methyl-*β*-cyclodextrin for 1 hour or cholesterol repletion with a cholesterol/cyclodextrin mixture (final concentration of cholesterol = 16 μg/ml) for another hour did not significantly affect the activation of NF-κB compared to control. Similarly, incubation of HuH-7 cells with rHDL for 16 hours or rHDL for 16 hours followed by cholesterol repletion for another hour with the cholesterol/cyclodextrin mixture also had no effect on the activation of NF-κB as measured by a NF-κB nuclear translocation assay.

rHDLs are more effective than 5 mmol/l salicylate at inhibiting TNFα-induced NF-κB activity

Sodium salicylate suppresses hepatic NF-κB activity and improves insulin sensitivity in C57BL/6 mice (22). We found that pre-treatment of the cells with rHDLs is as effective as 5 mmol/l sodium salicylate in suppressing TNF-α-activated NF-κB activation. HuH-7 cells were transfected with the NF-κB-luciferase reporter vector and then exposed to rHDLs (final apoAI concentration, 16 μmol/l = 0.45 mg/ml) or 5 mmol/l sodium salicylate (S) for 16 hours prior to a 5 hour TNF-α activation. Fig. 7A shows rHDLs suppressed TNF-α-induced NF-κB activation to levels similar to those observed with both 5 mmol/l sodium salicylate and the IKK inhibitor, Wedelolactone. Additionally, unlike 5 mmol/l sodium salicylate, rHDL treatment had no effect on cell viability (Fig. 7B).

rHDLs inhibit NF-κB target gene expression

NF-κB is a central mediator of the inflammatory response in many cell types (20, 21). Using a NF-κB target gene macroarray, it was determined that pre-treatment with rHDLs decreased the expression of a number of target genes, including cytokines/chemokines (*IL8, MCP1, PTX3, GRO1, SAA1*), proteinase inhibitors (*A1AT*), cell differentiation and proliferation associated genes (*GAL3, MAD3, TP53, PRG1*), reactive oxygen stress associated genes (*MNSOD, GSTP1*) and cell adhesion molecules (*LAMB2*)(ESM Fig. V). The macroarray results were confirmed by RT-qPCR (Table 2).

DISCUSSION

High fat feeding of mice induces systemic and hepatic inflammation, increases hepatic NF-κB activation, impairs glucose tolerance and induces insulin resistance (4, 23). The present study shows that intravenous infusion of apoAI into these animals reversed all of these changes. *In vitro*, TNF-α induced inflammation of hepatocytes resulted in increased IKK activity, increased phosphorylation of IκB-α and increased activation of NF-κB. Exposure of these activated hepatocytes to apoAI (as a component of rHDLs) reversed all of these changes.

The present study is the first to show that administration of apoAI is able to improve glucose tolerance and insulin sensitivity in HFD-fed C57BL/6 mice. The proposed mechanism involves anti-inflammatory effects via suppression of hepatic NF-κB activation. This mechanism is similar to that described for sodium salicylate in protecting against hepatic inflammatory and subsequently development of insulin resistance (4). Insulin resistance remains hard to treat as to date there are a few targeted medicines. We have previously demonstrated that rHDLs (with apoAI as the main protein) have strong anti-inflammatory effects in endothelial cells – a key cell type in atherosclerosis (12). Given that preparations of HDLs are currently in clinical development as anti-atherogenic agents, a logical next step will be to test the ability of these preparations in protecting against the hepatic inflammation and insulin resistance that accompanies non-alcoholic fatty liver.

In this study we showed that apoAI treatment, either independently or as part of a reconstituted HDL particle, suppressed a number of inflammatory, oxidant and apoptotic stimuli via signalling through the canonical NF-κB pathway. In previous studies, we have shown that administration of apoAI at a dosage of 8mg/kg does not lead to a significant increase in the circulating HDL level (24) and, as such, the molecular

mechanism activated *in vivo* by an apoAI injection to mediate the anti-inflammatory effects on hepatic NF-κB activation remains to be determined, although may involve upregulation of DHCR24 and other cellular protective enzymes. We have previously shown that apoAI as a component of discoidal rHDLs suppressed NF-κB activation through increased expression of DHCR24 (a cellular protective enzyme) levels, and that this enzyme is at least, in part, responsible for mediating the anti-inflammatory effects of rHDLs in human coronary aortic endothelial cells (12). However, in the current study, there was no increase in DHCR24 expression, at least at the mRNA level, in the liver of apoAI-treated mice so it is likely another mechanism is responsible for HDLs protection against NF-κB activation. One of the major protective properties of HDL revolves around its ability to promote cholesterol efflux. It has been shown in macrophages, endothelial cells and recently adipocytes (25–27) that the anti-inflammatory effects mediated by HDL is due, at least in part, to cholesterol efflux. However, in this study, we found that modulation of membrane cholesterol using methyl-β-cyclodextrin (depletes membrane cholesterol) or HDL had no effect on NF-κB activation suggesting that cholesterol efflux does not have a key role in the anti-inflammatory effects of HDL in hepatocytes. The underlying mechanism now needs to be interrogated further for a complete understanding.

We have also shown that 2- and 4-weeks of apoAI treatment decreased expression of the gluconeogenesis-associated PEPCK and G6Pase, an effect that correlated with an improved response to the pyruvate challenge. Thus, in addition to the effects on insulin resistance, apoAI may decrease glucose output from the liver via suppression of gluconeogenesis, most likely through effects on NF-κB.

Improvement in systemic insulin resistance and glucose homeostasis as a result of apoAI treatment may be an additive consequence of effects on multiple organs

including the liver, pancreas, adipose tissue and skeletal muscle. We have previously reported that apoAI treatment of cultured pancreatic β-cells increased both the synthesis and secretion of insulin in the setting of both high and low glucose concentrations (28). In keeping with this finding, apoAI as a component of rHDL has also been shown to reduce plasma glucose levels in patients with type 2 diabetes, associated with an rHDL mediated increase in plasma insulin (28). ApoAI rHDL was shown to increase AMPK activity in skeletal muscle in type 2 diabetes patients (29) and that this was a key pathway to glucose reduction in these patients as increased AMPK induces increased glucose uptake by skeletal muscle cells. In a study of apoAI-transgenic mice, rather than apoAI treatment, it was shown that adipose tissue inflammation induced by a high fat, high sucrose diet was ameliorated, relative to wild type mice, in keeping with reports that HDL and apoAI have anti-inflammatory effects on adipocytes (30). A direct anti-obesity effect on apoAI and its mimetic peptide has also been recently reported whereby HDL treatment increased adipose tissue expenditure through attainment of brown adipocyte phenotype in white adipose tissue (31). Apolipoprotein A-I possesses an anti-obesity effect associated with increase of energy expenditure and up-regulation of UCP1 in brown fat. We now show that apoAI decreases liver inflammation by suppressing NF-κB activation. It is likely that the profound ability of apoAI as a component of rHDL to improve insulin resistance is a combined effect on the liver, adipose tissue, pancreas and skeletal muscle. We suspect that apoAI-induced suppression of hepatic NF-κB activation is central to the overall protective effect of apoAI on insulin resistance, a suggestion consistent with the observations of Shoelson *et al* who demonstrated that NF-κB activation alone in the liver is sufficient to drive the onset of insulin resistance in mice (4).

A limitation of this study is that it was completed in a mouse model and therefore may not reflect what is clinically relevant in human subjects. However, recent findings in humans show that HDL-raising interventions were associated with an increase in insulin sensitivity in patients with type 2 diabetes (32). More direct evidence of HDL improving insulin resistance in humans was provided in a study showing infusion of rHDL particles increased increased plasma insulin levels, and decreased plasma glucose levels in type 2 diabetic subjects (29). Moreover, salsalate, a non-acetylated salicylate, was used to treat patients with type 2 diabetes and in this study reduced HbA1c levels (33) thereby providing evidence for the hypothesis that an anti-inflammatory approach could be used to treat insulin resistance and subsequent type 2 diabetes. However, to date, the mechanisms by which HDL improve insulin sensitivity in humans, and whether it involves anti-inflammatory effects as we have now demonstrated in C57BL/6 mice, remains to be investigated.

In summary, our findings that apoAI can improve insulin sensitivity through anti-inflammatory effects in hepatocytes may lead to novel approaches for the treatment of insulin resistance. We have shown that apoAI as a component of rHDLs potently suppresses the key mediator of inflammation, NF-κB, and in doing so can decrease the hepatic inflammation that underlies the onset of insulin resistance. HDL cholesterol levels are often reduced as a consequence of insulin resistance (13, 34). The results from this study, therefore, have important therapeutic implications whereby raising HDL levels have the potential to protect against hepatic inflammation, and subsequently, insulin resistance.

ACKNOWLEDGEMENTS AND DISCLOSURES

Grant support

This work was supported by University of Technology, Sydney Chancellor's Postdoctoral Research Fellowship Scheme and the Diabetes of Australia Research Trust.

Disclosures

None

REFERENCES

1. Shoelson, S. E., J. Lee, and A. B. Goldfine. 2006. Inflammation and insulin resistance. *J Clin Invest*. **116**: 1793–1801.
2. Muriel, P. 2009. NF-kB in liver diseases : a target for drug therapy. *Journal of applied toxicology : JAT*. **29**: 91–100.
3. Lawrence, T. 2009. The nuclear factor NF-kappaB pathway in inflammation. *Cold Spring Harbor perspectives in biology*. **1**: a001651.
4. Cai, D., M. Yuan, D. F. Frantz, P. A. Melendez, L. Hansen, J. Lee, and S. E. Shoelson. 2005. Local and systemic insulin resistance resulting from hepatic activation of IKK-beta and NF-kappaB. *Nat Med*. **11**: 183–190.
5. Hotamisligil, G. S. 2003. Inflammatory pathways and insulin action. *Int J Obes Relat Metab Disord*. **27 Suppl 3**: S53–5.
6. Karin, M., and M. Delhase. 2000. The I kappa B kinase (IKK) and NF-kappa B: key elements of proinflammatory signalling. *Seminars in immunology*. **12**: 85–98.
7. Hayden, M. S., and S. Ghosh. 2004. Signaling to NF-kappaB. *Genes & development*. **18**: 2195–224.
8. Baeuerle, P. A., and D. Baltimore. 1988. I kappa B: a specific inhibitor of the NF-kappa B transcription factor. *Science (New York, N.Y.)*. **242**: 540–6.
9. Ghosh, S., and D. Baltimore. 1990. Activation in vitro of NF-kappa B by phosphorylation of its inhibitor I kappa B. *Nature*. **344**: 678–82.
10. Nicholls, S. J., G. J. Dusting, B. Cutri, S. Bao, G. R. Drummond, K. A. Rye, and P. J. Barter. 2005. Reconstituted high-density lipoproteins inhibit the acute pro-oxidant and proinflammatory vascular changes induced by a periarterial collar in normocholesterolemic rabbits. *Circulation*. **111**: 1543–1550.
11. Murthy, S. N., C. V Desouza, N. W. Bost, R. S. Hilaire, D. B. Casey, A. M. Badejo, J. S. Dhaliwal, J. Mcgee, D. B. Mcnamara, P. J. Kadowitz, and V. A. Fonseca. 2010. Effects of Salsalate Therapy on Recovery From Vascular Injury in Female Zucker Fatty Rats. **59**.
12. McGrath, K. C., X. H. Li, R. Puranik, E. C. Liong, J. T. Tan, V. M. Dy, B. A. DiBartolo, P. J. Barter, K. A. Rye, and A. K. Heather. 2009. Role of 3beta-hydroxysteroid-delta 24 reductase in mediating antiinflammatory effects of high-density lipoproteins in endothelial cells. *Arterioscler Thromb Vasc Biol*. **29**: 877–882.
13. Karhapää, P., M. Malkki, and M. Laakso. 1994. Isolated low HDL cholesterol. An insulin-resistant state. *Diabetes*. **43**: 411–7.
14. Weisweiler, P. 1987. Isolation and quantitation of apolipoproteins A-I and A-II from human high-density lipoproteins by fast-protein liquid chromatography. *Clinica chimica acta; international journal of clinical chemistry*. **169**: 249–54.
15. Matz, C. E., and A. Jonas. 1982. Micellar complexes of human apolipoprotein A-I with phosphatidylcholines and cholesterol prepared from cholate-lipid dispersions. *J Biol Chem*. **257**: 4535–4540.
16. Ramírez-Zacarías, J. L., F. Castro-Muñozledo, and W. Kuri-Harcuch. 1992. Quantitation of adipose conversion and triglycerides by staining intracytoplasmic lipids with Oil red O. *Histochemistry*. **97**: 493–7.
17. Dean, R. T., W. Hylton, and A. C. Allison. 1979. Induction of macrophage lysosomal enzyme secretion by agents acting on the plasma membrane. *Exp Cell Biol*. **47**: 454–462.
18. Death, A. K., K. C. Y. McGrath, M. A. Sader, S. Nakhla, W. Jessup, D. J. Handelsman, and D. S. Celermajer. 2004. Dihydrotestosterone promotes vascular cell adhesion

molecule-1 expression in male human endothelial cells via a nuclear factor-kappaB-dependent pathway. *Endocrinology*. **145**: 1889–97.
19. Bustin, S. A. 2000. Absolute quantification of mRNA using real-time reverse transcription polymerase chain reaction assays. *Journal of molecular endocrinology*. **25**: 169–93.
20. Pahl, H. L. 1999. Activators and target genes of Rel/NF-kappaB transcription factors. *Oncogene*. **18**: 6853–66.
21. Oeckinghaus, A., and S. Ghosh. 2009. The NF-kappaB family of transcription factors and its regulation. *Cold Spring Harbor perspectives in biology*. **1**: a000034.
22. Kopp, E., and S. Ghosh. 1994. Inhibition of NF-kappa B by sodium salicylate and aspirin. *Science*. **265**: 956–959.
23. Arkan, M. C., A. L. Hevener, F. R. Greten, S. Maeda, Z. W. Li, J. M. Long, A. Wynshaw-Boris, G. Poli, J. Olefsky, and M. Karin. 2005. IKK-beta links inflammation to obesity-induced insulin resistance. *Nat Med*. **11**: 191–198.
24. Reimers, G. J., C. L. Jackson, J. Rickards, P. Y. Chan, J. S. Cohn, K.-A. Rye, P. J. Barter, and K. J. Rodgers. 2011. Inhibition of rupture of established atherosclerotic plaques by treatment with apolipoprotein A-I. *Cardiovascular research*. **91**: 37–44.
25. Yvan-Charvet, L., C. Welch, T. a Pagler, M. Ranalletta, M. Lamkanfi, S. Han, M. Ishibashi, R. Li, N. Wang, and A. R. Tall. 2008. Increased inflammatory gene expression in ABC transporter-deficient macrophages: free cholesterol accumulation, increased signaling via toll-like receptors, and neutrophil infiltration of atherosclerotic lesions. *Circulation*. **118**: 1837–47.
26. Sun, Y., M. Ishibashi, T. Seimon, M. Lee, S. M. Sharma, K. a Fitzgerald, A. O. Samokhin, Y. Wang, S. Sayers, M. Aikawa, W. G. Jerome, M. C. Ostrowski, D. Bromme, P. Libby, I. a Tabas, C. L. Welch, and A. R. Tall. 2009. Free cholesterol accumulation in macrophage membranes activates Toll-like receptors and p38 mitogen-activated protein kinase and induces cathepsin K. *Circulation research*. **104**: 455–65.
27. Murphy, A. J., K. J. Woollard, A. Hoang, N. Mukhamedova, R. a Stirzaker, S. P. a McCormick, A. T. Remaley, D. Sviridov, and J. Chin-Dusting. 2008. High-density lipoprotein reduces the human monocyte inflammatory response. *Arteriosclerosis, thrombosis, and vascular biology*. **28**: 2071–7.
28. Fryirs, M. A., P. J. Barter, M. Appavoo, B. E. Tuch, F. Tabet, A. K. Heather, and K. A. Rye. Effects of high-density lipoproteins on pancreatic beta-cell insulin secretion. *Arterioscler Thromb Vasc Biol*. **30**: 1642–1648.
29. Drew, B. G., S. J. Duffy, M. F. Formosa, A. K. Natoli, D. C. Henstridge, S. A. Penfold, W. G. Thomas, N. Mukhamedova, B. de Courten, J. M. Forbes, F. Y. Yap, D. M. Kaye, G. van Hall, M. A. Febbraio, B. E. Kemp, D. Sviridov, G. R. Steinberg, and B. A. Kingwell. 2009. High-density lipoprotein modulates glucose metabolism in patients with type 2 diabetes mellitus. *Circulation*. **119**: 2103–11.
30. Umemoto, T., C. Y. Han, P. Mitra, M. M. Averill, C. Tang, L. Goodspeed, M. Omer, S. Subramanian, S. Wang, L. J. Den Hartigh, H. Wei, E. J. Kim, J. Kim, K. D. O'Brien, and A. Chait. 2013. Apolipoprotein AI and high-density lipoprotein have anti-inflammatory effects on adipocytes via cholesterol transporters: ATP-binding cassette A-1, ATP-binding cassette G-1, and scavenger receptor B-1. *Circulation research*. **112**: 1345–54.
31. Ruan, X., Z. Li, Y. Zhang, L. Yang, Y. Pan, Z. Wang, G.-S. Feng, and Y. Chen. 2011. Apolipoprotein A-I possesses an anti-obesity effect associated with increase of energy expenditure and up-regulation of UCP1 in brown fat. *Journal of cellular and molecular medicine*. **15**: 763–72.

32. Barter, P. J., K.-A. Rye, J.-C. Tardif, D. D. Waters, S. M. Boekholdt, A. Breazna, and J. J. P. Kastelein. 2011. Effect of torcetrapib on glucose, insulin, and hemoglobin A1c in subjects in the Investigation of Lipid Level Management to Understand its Impact in Atherosclerotic Events (ILLUMINATE) trial. Circulation. 124: 555–62.
33.Goldfine AB, Fonseca V, Jablonski KA et al. 2010 The effects of salsalate on glycemic control in patients with type 2 diabetes: a randomized trial. Ann Intern Med 152:346–357
34. Tai, E., S. C. Emmanuel, S. Chew, B. Tan, and C. Ta. 1999. An Insulin-Resistant State Only in the Presence of Fasting. **48**: 1088–1092.

FIGURE LEGENDS

Fig. 1: Body weights of C57BL/6 mice and hepatic mRNA levels of genes involved in fat synthesis.

(A) Beginning at 6 weeks of age, C57BL/6 mice were fed a standard chow diet (StD) or high-fat diet (HFD) for 16 wk. The HFD group was subdivided: HFD was administered endotoxin-free PBS for the last 4 week of diet; HFD+2wk apoAI was administered apoAI for the last 2 week of diet and HFD+4wk apoAI was administered apoAI for the last 4 week of diet. Body weight was monitored once weekly (n=10 for each treatment group). **p*<0.001 vs. StD.

(B) *SREBP-1* and **(C)** *ChREBP* mRNA levels were measured by qPCR. mRNA levels were normalized to *transcription factor IID* (*Tbp*). Results are mean ± SEM (n=8-10). $^{\#}p < 0.05$ vs. StD; **p*<0.05 vs. HFD

Fig. 2: Plasma glucose concentrations during metabolic assays in C57BL/6 mice fed a standard chow diet (StD) or a high fat diet (HFD) and treated with apoAI.

(A) Intraperitoneal glucose tolerance test (IPGTT; glucose 1g /kg) and **(B)** area under the curve for glucose (AUC glucose) was calculated using the trapezoid rule. **(C)** Intraperitoneal insulin tolerance test (IPITT; insulin 0.75 IU/kg) and **(D)** AUC glucose. **(E)** Pyruvate (pyruvate 2 g/kg) challenge test and **(F)** AUC glucose. Results are mean ± SEM (n=8-10). †*p*<0.05 vs. StD; **p*< 0.05 vs. HFD.

Fig. 3: Serum cytokine levels in C57BL/6 mice treated with apoA-I.

C57BL/6 mice were fed a standard chow diet (StD) or a high fat diet (HFD) and treated with apoAI as described in the methods. Circulating levels of TNF-α **(A)**, IL-6 **(B)** and IFN-γ **(C)**

were determined using the Bioplex kit (Bio-Rad). Results are mean ± SEM (n=8-10). †p< 0.05 vs. StD; §p<0001 vs. StD; *p<0.05 vs. HFD; **p<0.01 vs. HFD.

Fig. 4: Administration of ApoAI decreases hepatic NF-κB activity.

C57BL/6 mice were fed a standard chow diet (StD) or a high fat diet (HFD) and treated with apoAI as described in the methods. Hepatic NF-κB activity was measured by an oligonucleotide specific for the NF-κB consensus DNA sequence. Results are means ± SEM (n=8-10). †p< 0.05 vs. StD; *p<0.05 vs. HFD.

Fig. 5: rHDLs suppress TNFα-activated signalling through the classical NF-κB pathway.

(A) HuH-7 cells transfected with an NF-κB-luciferase reporter vector. Transfected cells were treated with PBS (control), TNF-α, pre-incubated with rHDLs (final apoAI concentration 16 μmol/l or 0.45 mg/ml) then stimulated with TNF-α (rHDL+TNFα) or pre-incubated with rHDLs for 16 hrs, and the rHDLs removed from the culture media prior to activation with TNF-α (rHDL//TNFα). Cells were then harvested, lysed and the cell lysates were assayed for luciferase activity. Results are expressed as mean ± SEM (n=5). §p<0.001 vs. Control; ***p<0.001 vs. TNF-α.

(B) rHDLs suppress TNFα-induced translocation of NF-κB in hepatocytes. HuH-7 cells were treated with PBS (control), TNFα or pre-incubated with rHDLs (final apoAI concentration 16 μmol/l or 0.45 mg/ml) then stimulated with TNF-α (rHDL+TNFα). Nuclear proteins were extracted and NF-κB levels measured. Results are expressed as mean ± SEM (n=5). †p<0.05 vs. Control; ***p < 0.001 vs. TNF-α.

(C) rHDLs suppress TNF-α-activated IKK activity in hepatocytes. HuH-7 cells were pre-treated with rHDLs (final apoAI concentration 16 μmol/l or 0.45 mg/ml) or PBS (control) for 16 hrs then exposed to TNFα for 15 mins. Results are expressed as mean ± SEM (*n*=5). ‡$p<0.01$ vs. Control; *$p<0.05$ vs. TNF-α.

(D) rHDLs prevent degradation of IκBα in hepatocytes. HuH-7 cells were pre-incubated for 16 hrs with rHDLs (final apoAI concentration 16 μmol/l or 0.45 mg/ml) or PBS (control) then stimulated with TNF-α for 24 hours. Protein lysates were extracted and the level of phosphorylated IκBα measured by ELISA. Results are expressed as mean ± SEM (n=5). §$p<0.001$ vs. Control; ***$p<0.001$ vs. TNF-α.

Fig. 6: Cholesterol depletion/repletion has no effect on the activation of NF-κB.

Cholesterol depletion was performed on HuH-7 cells by incubation with 1.5% cyclodextrin (CD) for 1 hour. Cholesterol repletion was performed by the addition of CD plus cholesterol for a further 1 hour. To assess the effects of rHDL on cholesterol mobilisaton, cells were treated with rHDL (final apoAI concentration 16 μmol/l or 0.45 mg/ml) for 16 hours followed by the addition of CD plus cholesterol for a further 1 hour. Following incubations, nuclear proteins were extracted and NF-κB levels measured. Results are expressed as mean ± SEM (*n*=3).

Fig. 7: Inhibition of TNFα-induced NF-κB activity by rHDLs versus salicylate.

(A) HuH-7 cells were transfected with an NF-κB-luciferase reporter vector then pre-incubated for 16 hrs with PBS (control), rHDLs (final apoAI concentration 16 μmol/l or 0.45 mg/ml), sodium salicylate (5 mmol/l) or the IKK inhibitor, Wedelolactone, prior to stimulation with TNF-α for 5 hours. The cells were harvested, lysed and the cell lysates were

assayed for luciferase activity. Results are expressed as mean ± SEM (n=5). †p<0.05 vs. Control; *p<0.05 vs. TNF-α.

(B) HuH-7 cells were pre-incubated for 16 hrs with PBS (control), rHDLs (final apoAI concentration 16 μmol/l or 0.45 mg/ml) or salicylate (S, 5 mmol/l) for 40 hours. Cell viability was then measured by the lactate dehydrogenase assay. Results are expressed as mean ± SEM (n=5). *p<0.05 vs. Control. *NS* = not significant.

ELECTRONIC SUPPLEMENTARY MATERIAL FIGURE LEGENDS

ESM Fig. I: Insulin resistance in C57BL/6 mice treated with apoAI

HOMA-IR, homeostasis model assessment-insulin resistance

(fasting glucose (mmol/l) x fasting insulin (mU/L)/22.5). Results are mean ± SEM (n=8-10). †$p<0.05$ vs. StD; *$p<0.05$ vs. HFD

ESM Fig. II: Fasting blood glucose and serum insulin levels

C57BL/6 mice were fed a standard chow diet (StD) or a high fat diet (HFD) and treated with apoAI as described in the method section. Following an overnight fast, **(A)** serum insulin levels were determined by ELISA and **(B)** blood glucose levels were determined using a glucose meter. n=8-10 for each treatment group. †$p<0.05$ vs. StD; *$p<0.05$ vs. HFD

ESM Fig. III: Circulating triglyceride and hepatic neutral lipid (triglyceride and cholesterol esters) levels.

C57BL/6 mice were fed a standard chow diet (StD) or a high fat diet (HFD) and treated with apoAI as described in the method section. **(A)** Serum triglyceride levels were determined as described in the method section. **(B)** Intrahepatic neutral lipid (triglyceride plus cholesterol esters) accumulation was determined by Oil Red-O staining. n=8-10 for each treatment group. ‡$p<0.01$ vs. StD; *$p<0.05$ vs. HFD.

ESM Fig. IV: ApoAI does not affect hepatic expression of DHCR24 mRNA levels.

C57BL/6 mice were fed a standard chow diet (StD) or a high fat diet (HFD) and treated with apoAI as described in the method section. DHCR24 mRNA levels were measured by qPCR. mRNA levels were normalized to β2-microglobulin. Results are mean ± SEM (n=8-10).

ESM Fig. V: AI-rHDLs suppress TNFα-activated NF-κB target gene expression in HuH-7 cells.

HuH-7 cells were pre-incubated with AI-rHDLs (final apoAI concentration, 16 μmol/l or 0.45 mg/ml) or PBS (vehicle control) for 16 hrs then stimulated with TNFα for 5 hrs. **(A)** Representative macroarray images for PBS+TNFα and rHDL+TNFα treatments are shown. **(B)** Schematic diagram of the Human TranSignal NF-κB Target Gene Array (Panomics). The genes on the array are spotted in duplicate. For alignment purpose, biotinylated DNA has been spotted along the right and bottom sides of the array.

Table 1: Hepatic mRNA gene expression.

Beginning at 6 weeks of age, C57BL/6 mice were fed a standard chow (StD) or high-fat diet for 16 wk. The HFD group were divided into 3 groups and administered with apoAI (8 mg/kg) for 4 wk, 2 wk or endotoxin-free PBS (HFD). Total RNA was isolated from liver tissue and mRNA levels measured by RT-qPCR. All cytokine mRNA levels were normalised to *transcription factor IID* (Tbp). RT-qPCR data represent fold increase over StD or HFD. Results are means ± SEM (n=8-10). *p<0.05, **p<0.01, n=8-10 animal for each treatment group.

Encoded protein	HFD/StD	2 wk apoAI/HFD	4 wk apoAI/HFD
PEPCK	1.95 ± 1.94↑*	0.43 ± 0.57↓*	0.45 ± 0.70↓*
G6Pase	1.76 ± 3.10↑*	0.54 ± 0.84↓*	0.41 ± 0.53↓**
TNF-α	1.65 ± 4.00↑*	0.11 ± 0.10↓**	0.22 ± 0.17↓**
IL-6	1.33 ± 2.20↑*	0.49 ± 1.17↓**	0.30 ± 0.70↓**
IFN-γ	4.14 ± 3.10↑**	0.70 ± 0.66↓*	0.61 ± 1.00↓**
IL-1β	4.96 ± 6.11↑*	0.42 ± 0.25↓**	0.24 ± 0.19↓**
SAA1	21.06 ± 8.38↑**	0.51 ± 0.36↓*	0.25 ± 0.28↓**
CD68	4.43 ± 1.76↑**	0.64 ± 1.89↓*	0.58 ± 1.06↓*
F4/80	7.02 ± 5.87↑**	0.63 ± 1.46↓*	0.58 ± 0.99↓*

Figure 1

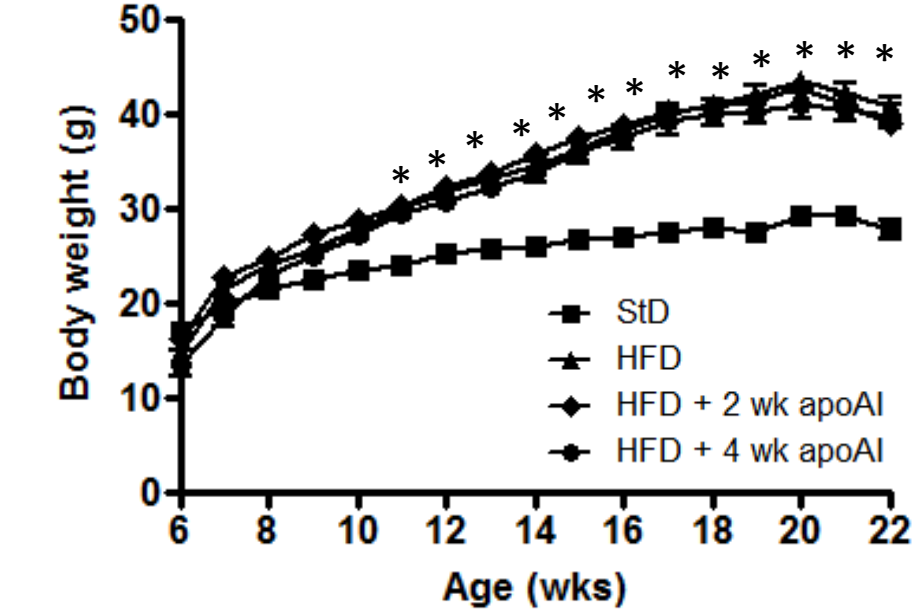
A
Body weight (g)
50
40
30
20
10
0
6
8
10
12
14
16
18
20
22
Age (wks)
StD
HFD
HFD + 2 wk apoAI
HFD + 4 wk apoAI
* * * * * * * * * * * *

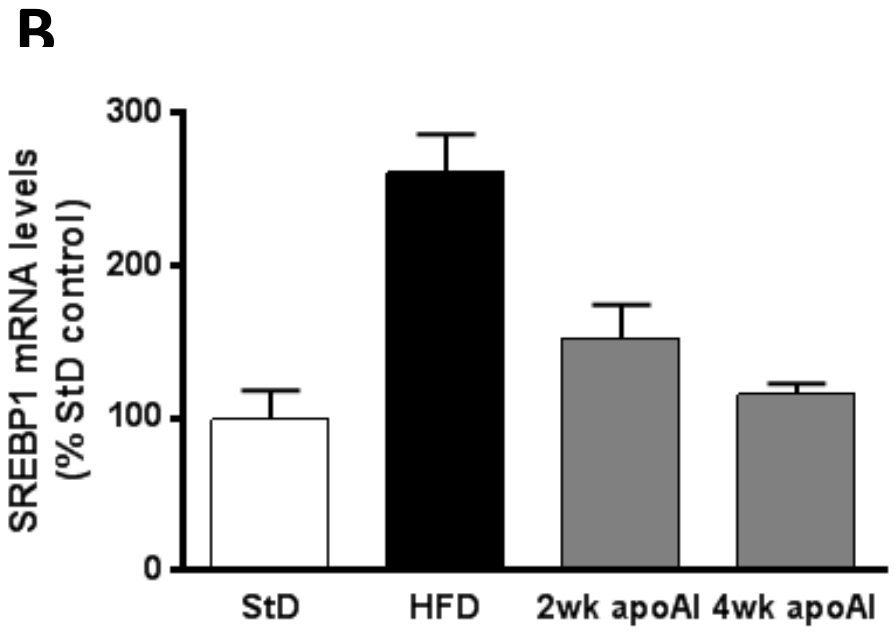
B
SREBP1 mRNA levels
(% StD control)
300
200
100
0
StD
HFD
2wk apoAI
4wk apoAI

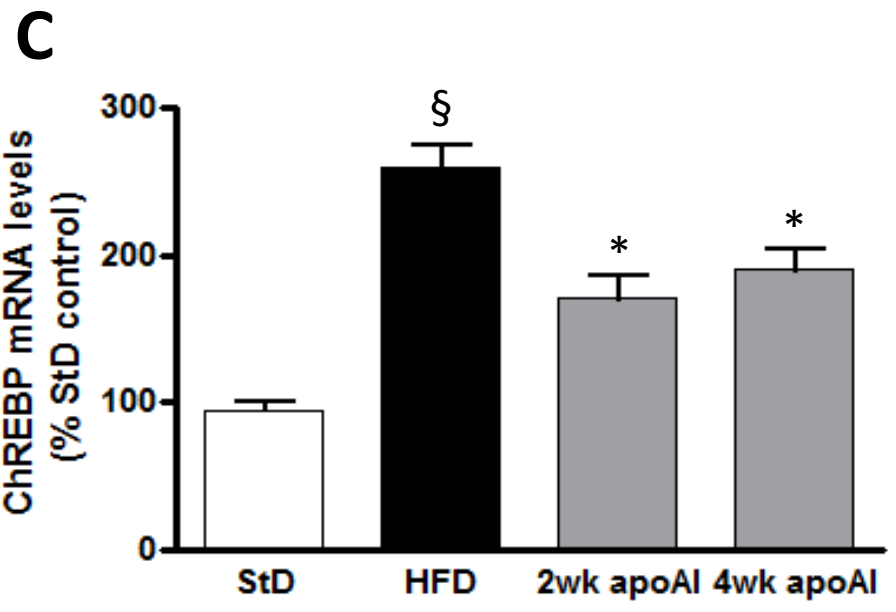
C
ChREBP mRNA levels
(% StD control)
300
200
100
0
§
*
*
StD
HFD
2wk apoAI
4wk apoAI

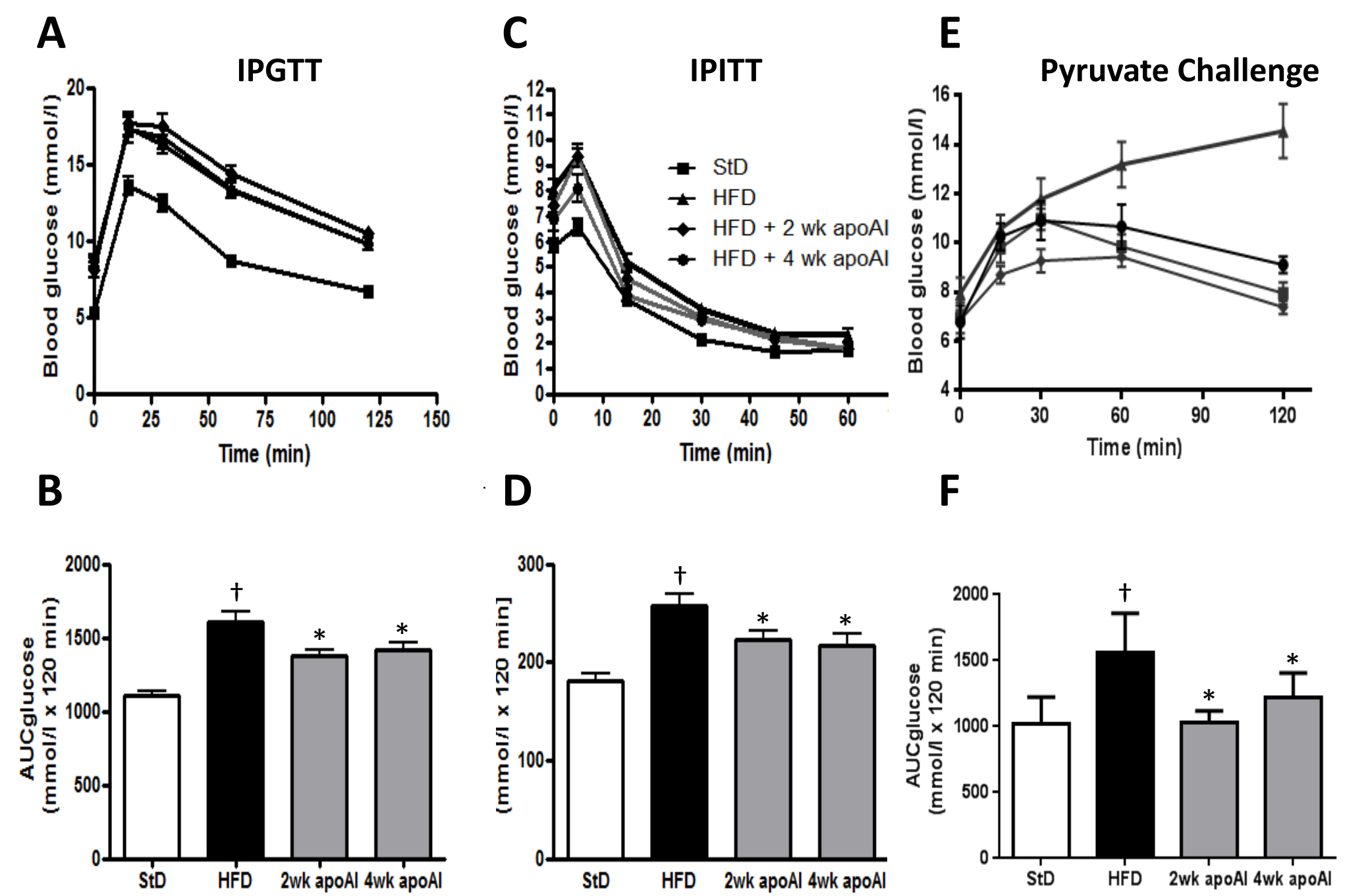
A
IPGTT
Blood glucose (mmol/l)
Time (min)
C
IPITT
StD
HFD
HFD + 2 wk apoAI
HFD + 4 wk apoAI
E
Pyruvate Challenge
B
AUCglucose (mmol/l x 120 min)
D
F
StD
HFD
2wk apoAI
4wk apoAI

Figure 2

Figure 3

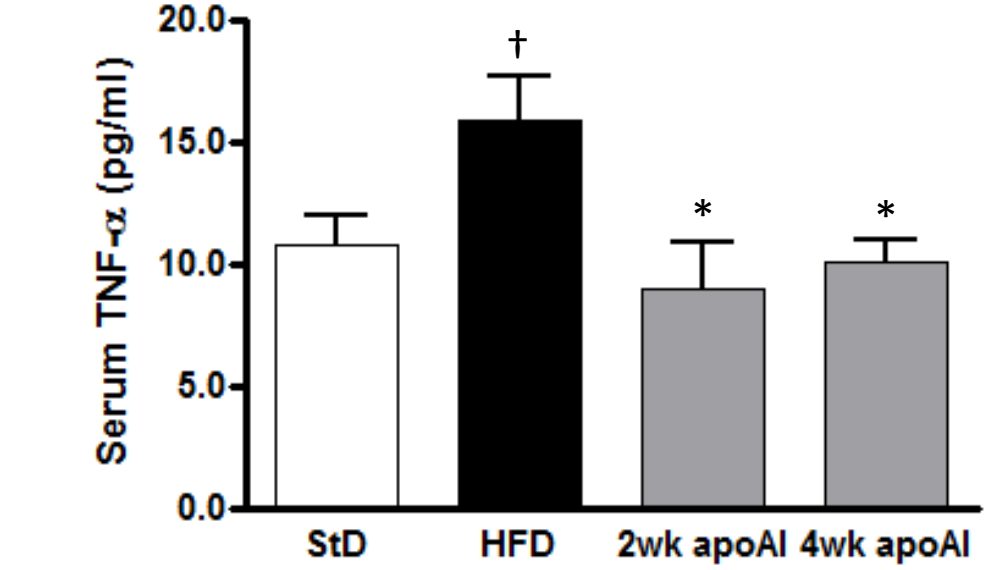
A
Serum TNF-α (pg/ml)
20.0
15.0
10.0
5.0
0.0
†
*
*
StD
HFD
2wk apoAI
4wk apoAI

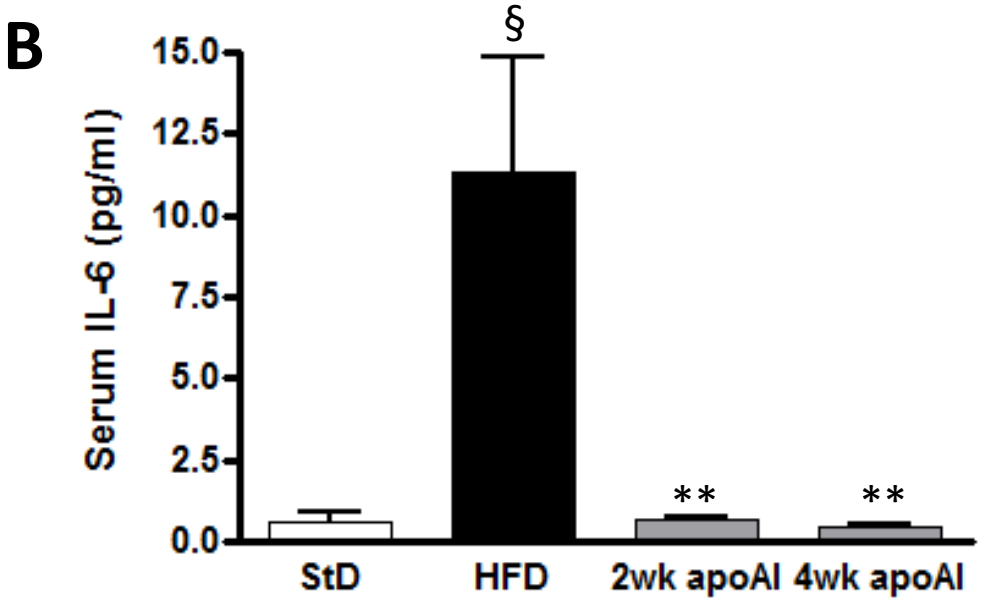
B
Serum IL-6 (pg/ml)
15.0
12.5
10.0
7.5
5.0
2.5
0.0
§
**
**
StD
HFD
2wk apoAI
4wk apoAI

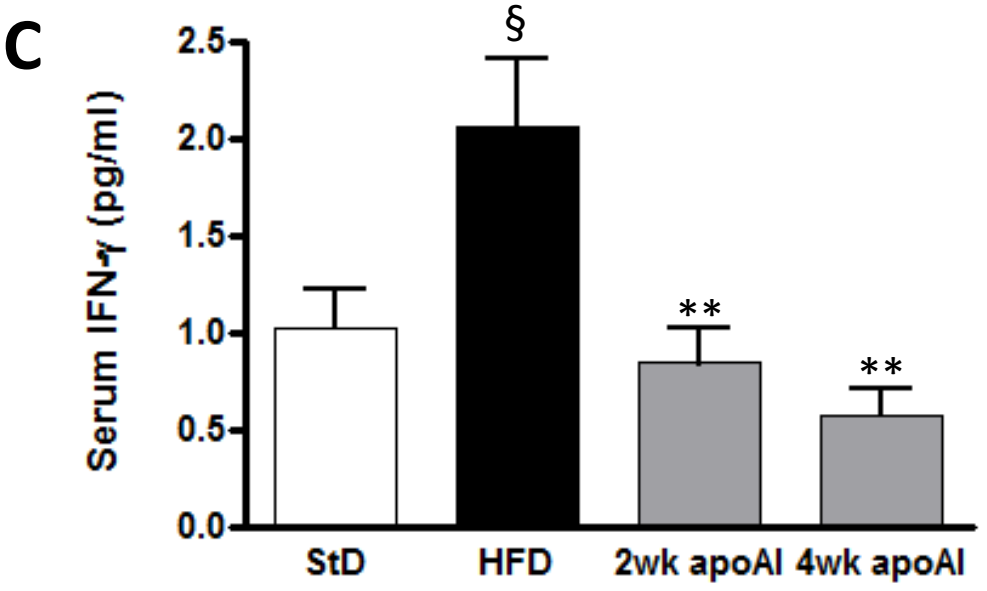
C
Serum IFN-γ (pg/ml)
2.5
2.0
1.5
1.0
0.5
0.0
§
**
**
StD
HFD
2wk apoAI
4wk apoAI

Figure 4

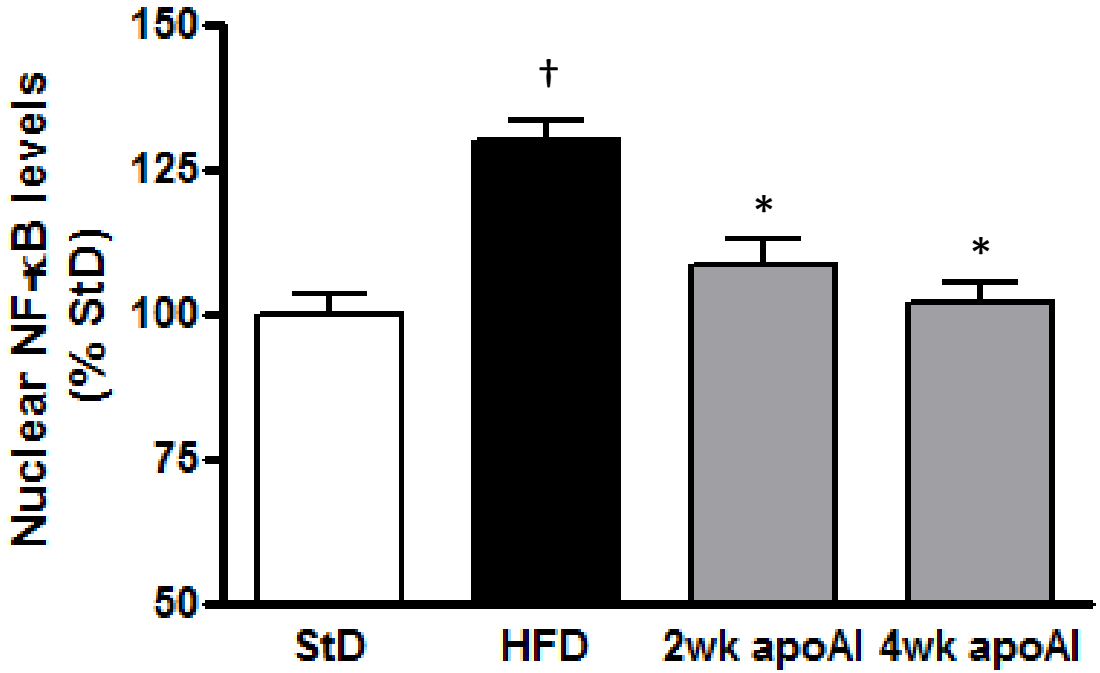
Nuclear NF-κB levels
(% StD)
150
125
100
75
50
†
*
*
StD
HFD
2wk apoAI
4wk apoAI

Figure 5

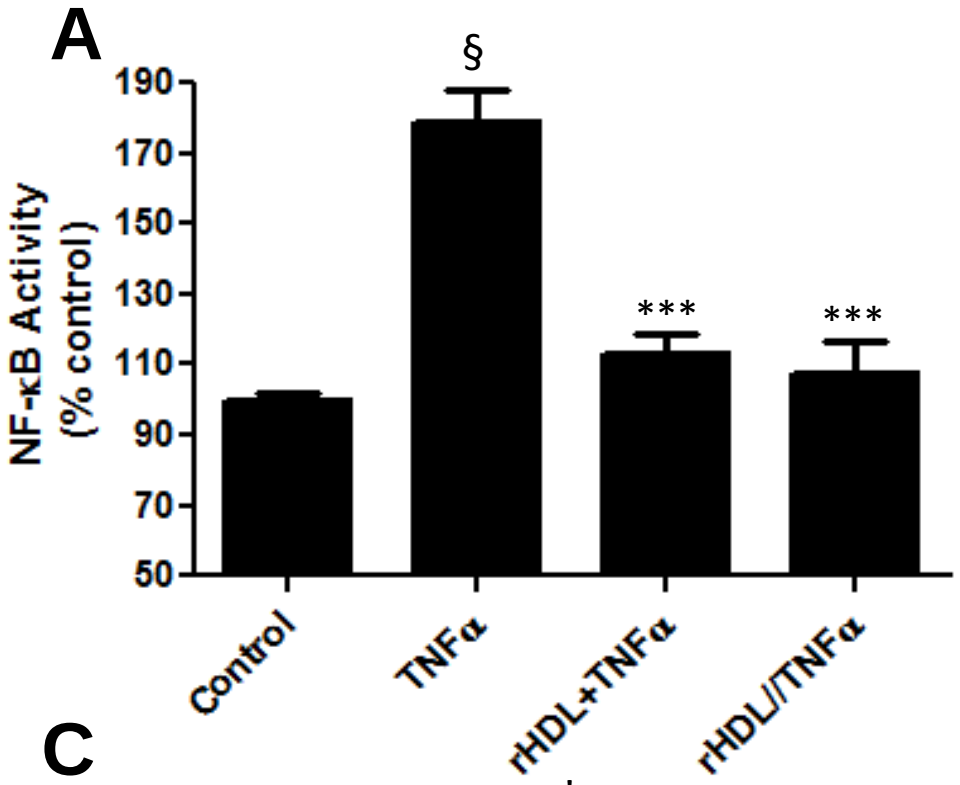
A
§
***
***
NF-κB Activity
(% control)
190
170
150
130
110
90
70
50
Control
TNFα
rHDL+TNFα
rHDL//TNFα

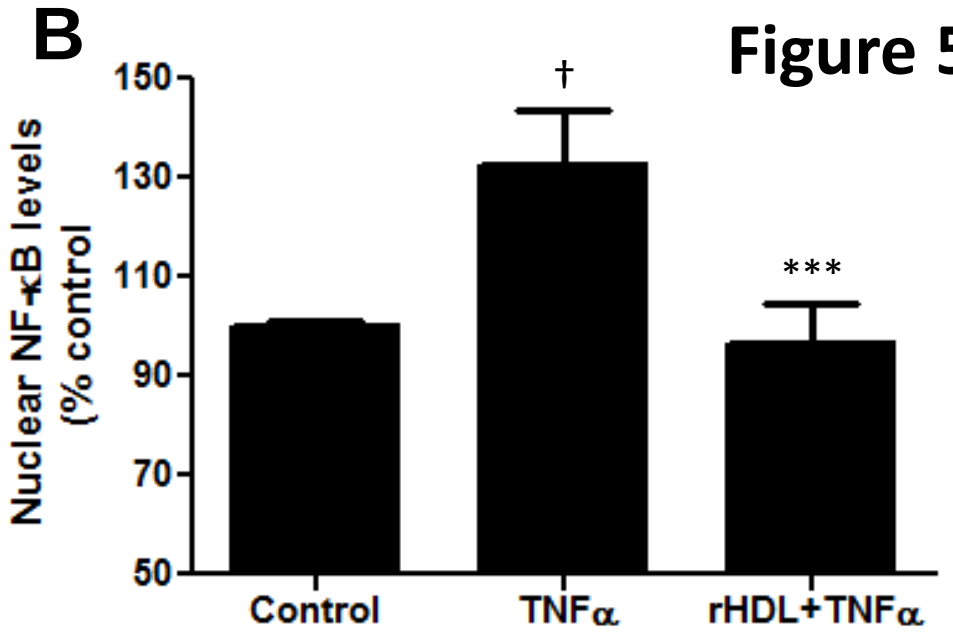
B
†
***
Nuclear NF-κB levels
(% control
150
130
110
90
70
50
Control
TNFα
rHDL+TNFα

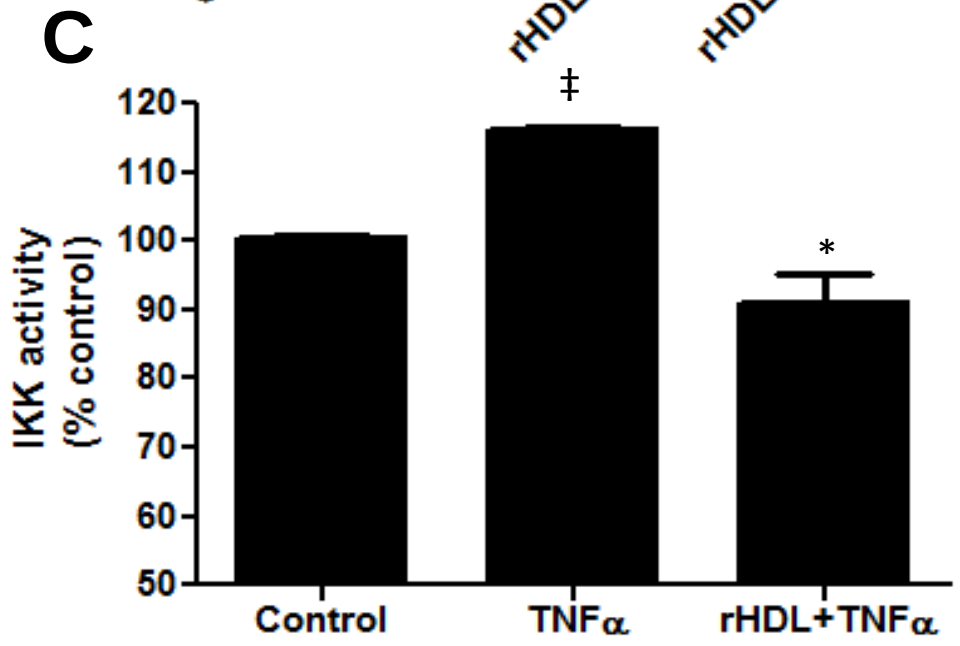
C
‡
*
IKK activity
(% control)
120
110
100
90
80
70
60
50
Control
TNFα
rHDL+TNFα

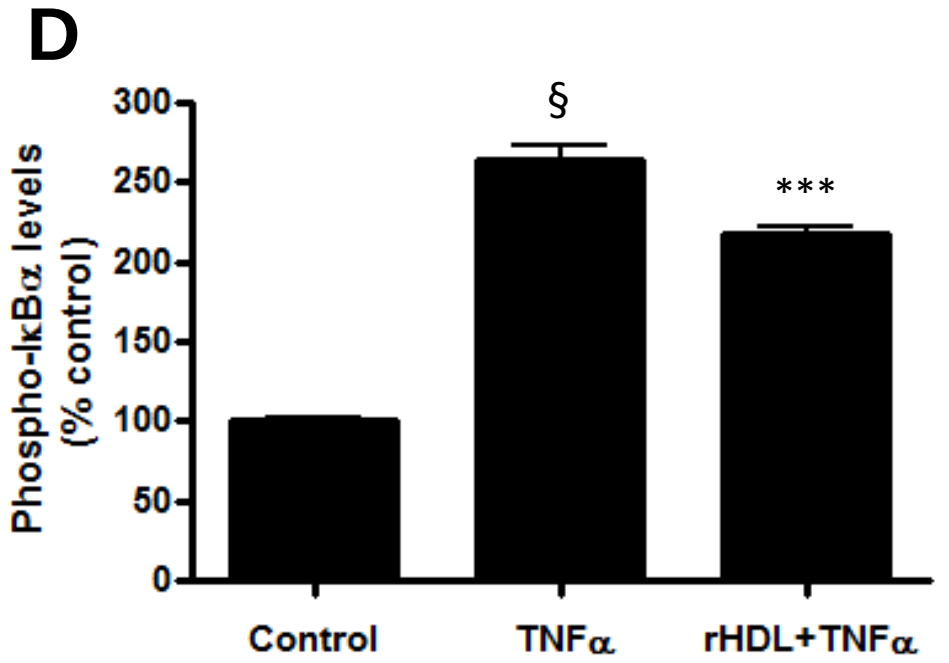
D
§
***
Phospho-IκBα levels
(% control)
300
250
200
150
100
50
0
Control
TNFα
rHDL+TNFα

Figure 6

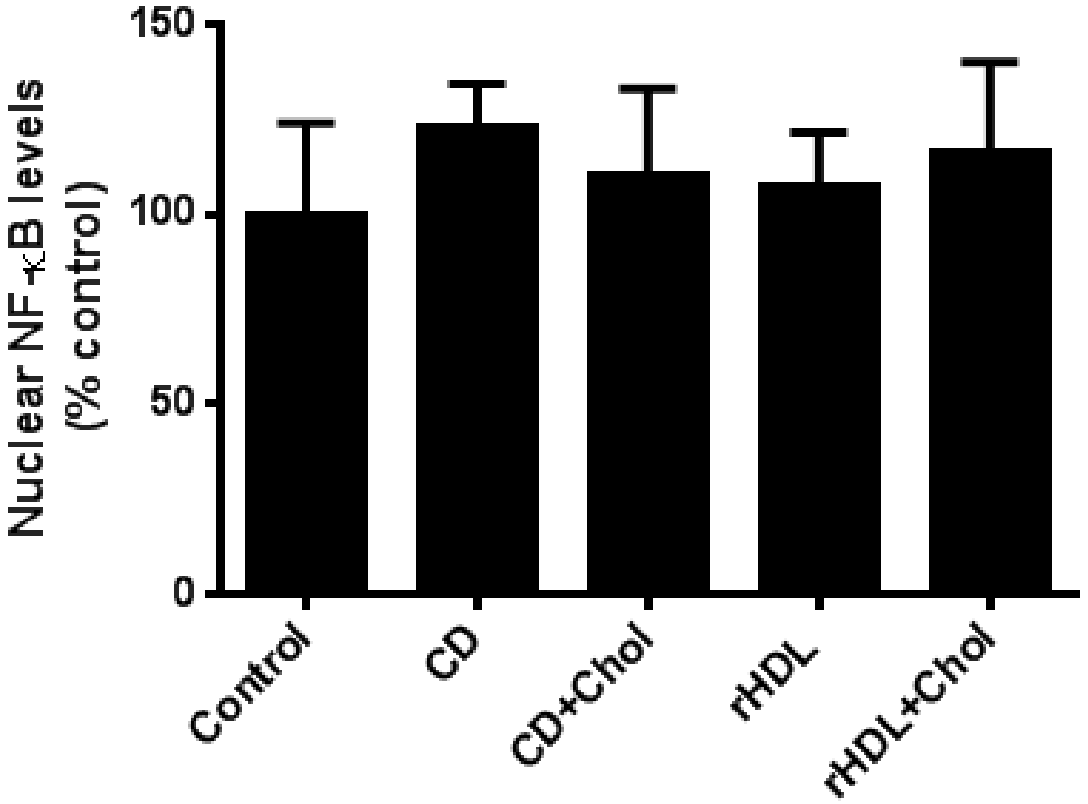
Nuclear NF-κB levels
(% control)
150
100
50
0
Control
CD
CD+Chol
rHDL
rHDL+Chol

Figure 7

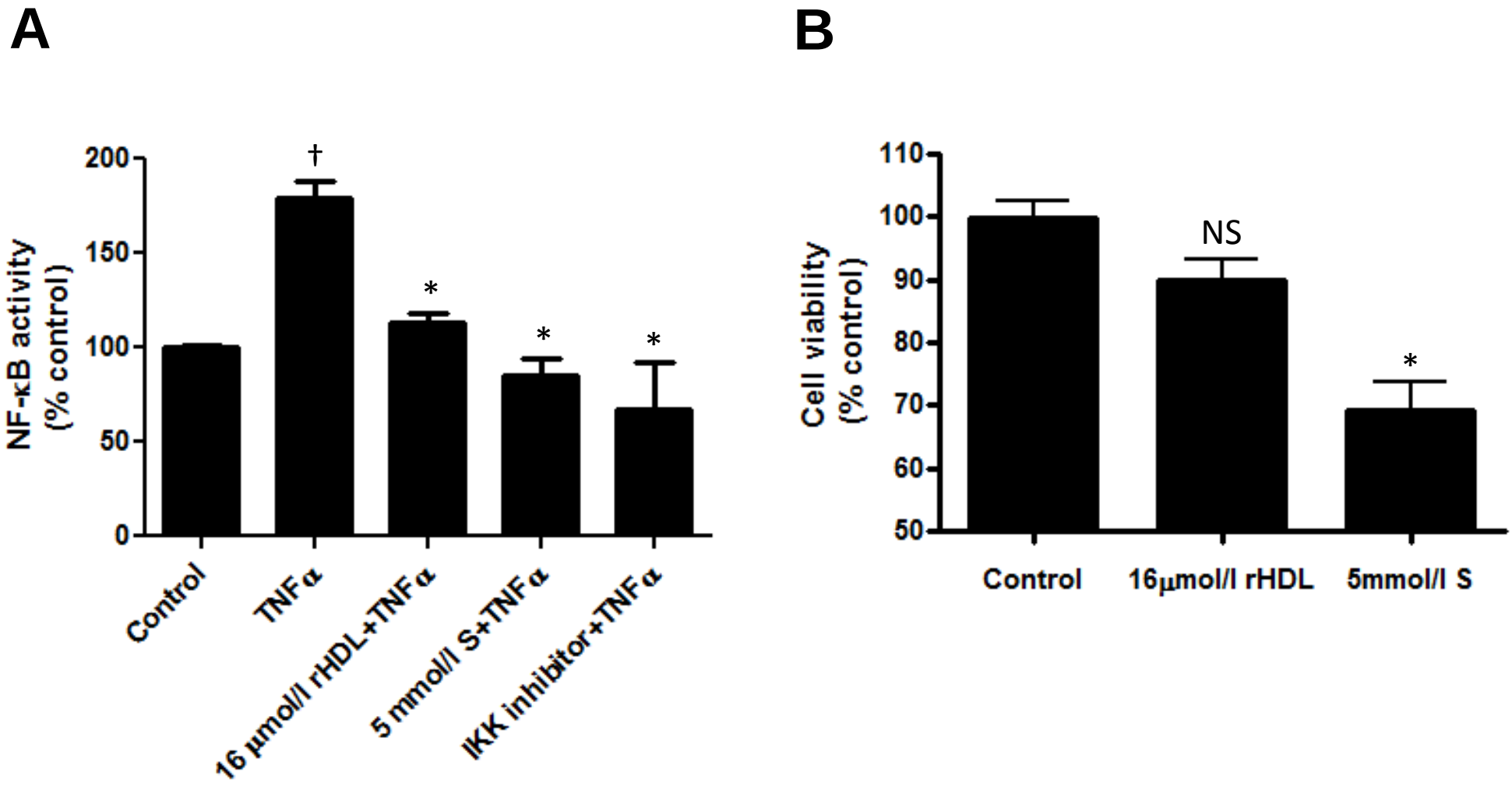
A
NF-κB activity (% control)
200
150
100
50
0
†
*
*
*
Control
TNFα
16 μmol/l rHDL+TNFα
5 mmol/l S+TNFα
IKK inhibitor+TNFα
B
Cell viability (% control)
110
100
90
80
70
60
50
NS
*
Control
16μmol/l rHDL
5mmol/l S

Figure 1

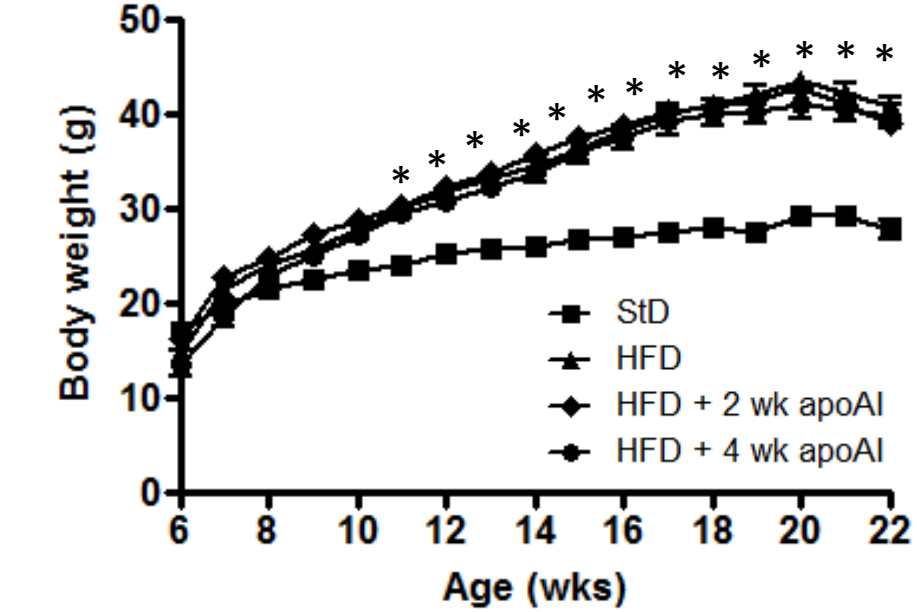
A
Body weight (g)
50
40
30
20
10
0
6
8
10
12
14
16
18
20
22
Age (wks)
StD
HFD
HFD + 2 wk apoAI
HFD + 4 wk apoAI
* * * * * * * * * * * *

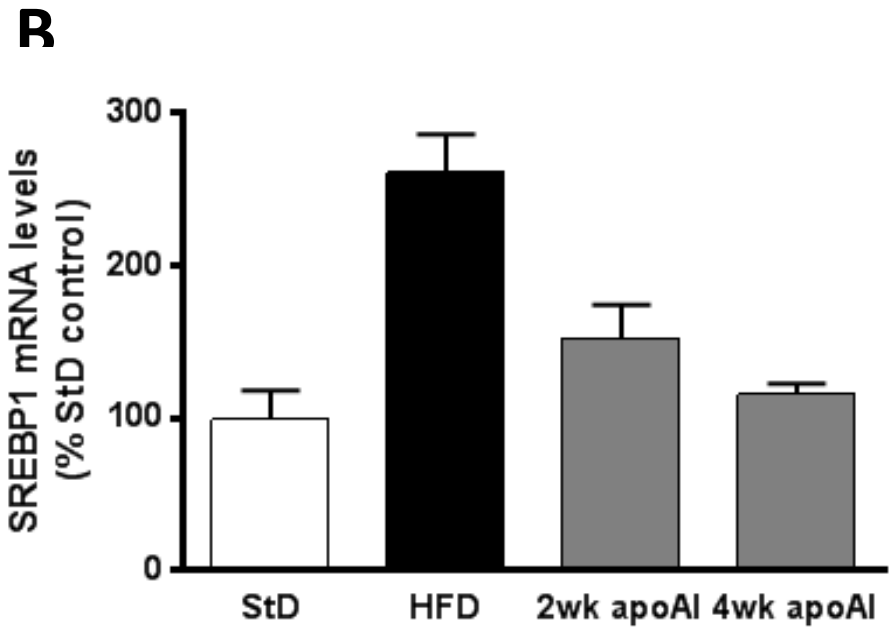
B
SREBP1 mRNA levels
(% StD control)
300
200
100
0
StD
HFD
2wk apoAI
4wk apoAI

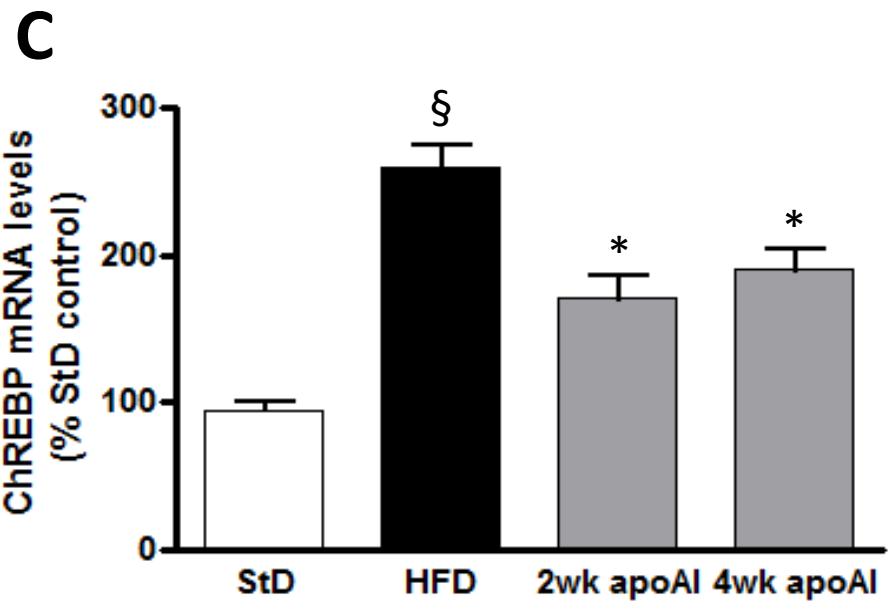
C
ChREBP mRNA levels
(% StD control)
300
200
100
0
§
*
*
StD
HFD
2wk apoAI
4wk apoAI

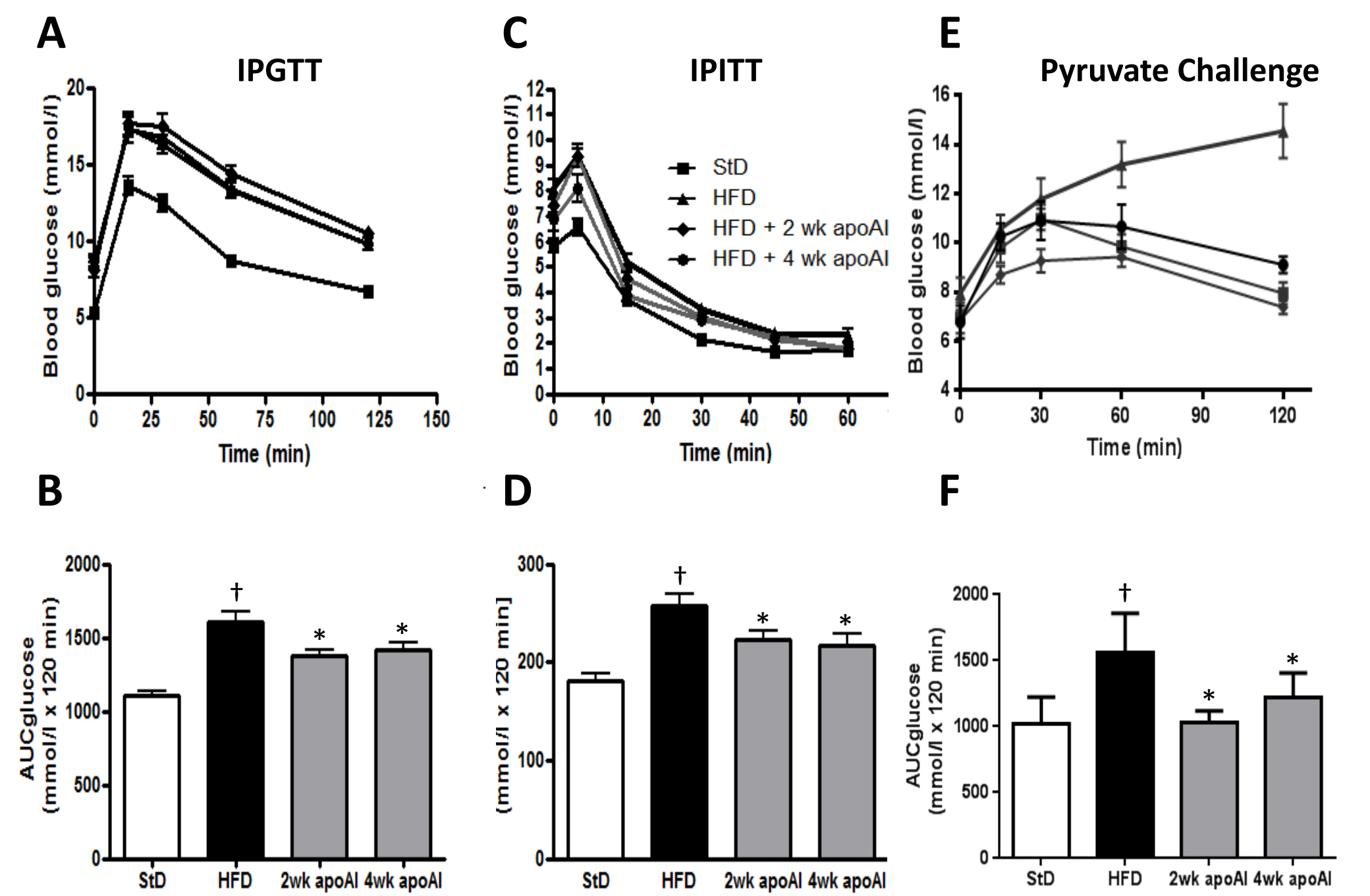
A
IPGTT
Blood glucose (mmol/l)
Time (min)
C
IPITT
StD
HFD
HFD + 2 wk apoAI
HFD + 4 wk apoAI
E
Pyruvate Challenge
B
AUCglucose (mmol/l x 120 min)
D
F
StD
HFD
2wk apoAI
4wk apoAI

Figure 2

Figure 3

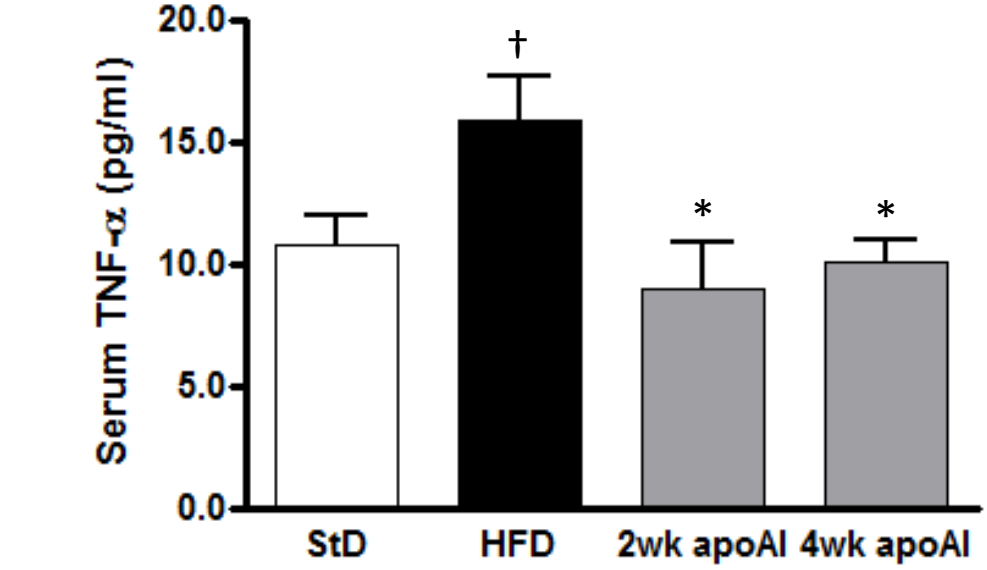
A
Serum TNF-α (pg/ml)
20.0
15.0
10.0
5.0
0.0
†
*
*
StD
HFD
2wk apoAI
4wk apoAI

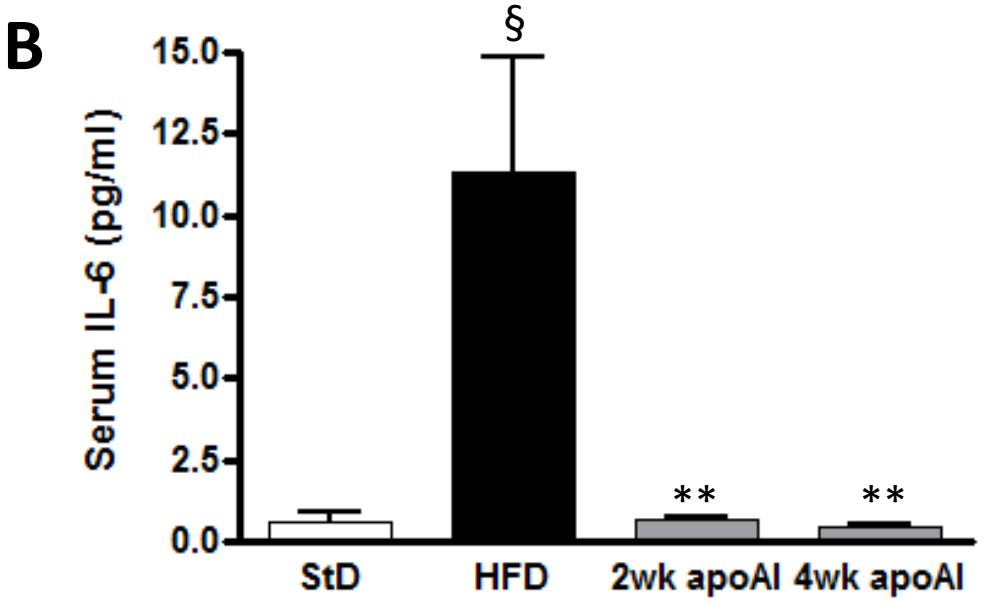
B
Serum IL-6 (pg/ml)
15.0
12.5
10.0
7.5
5.0
2.5
0.0
§
**
**
StD
HFD
2wk apoAI
4wk apoAI

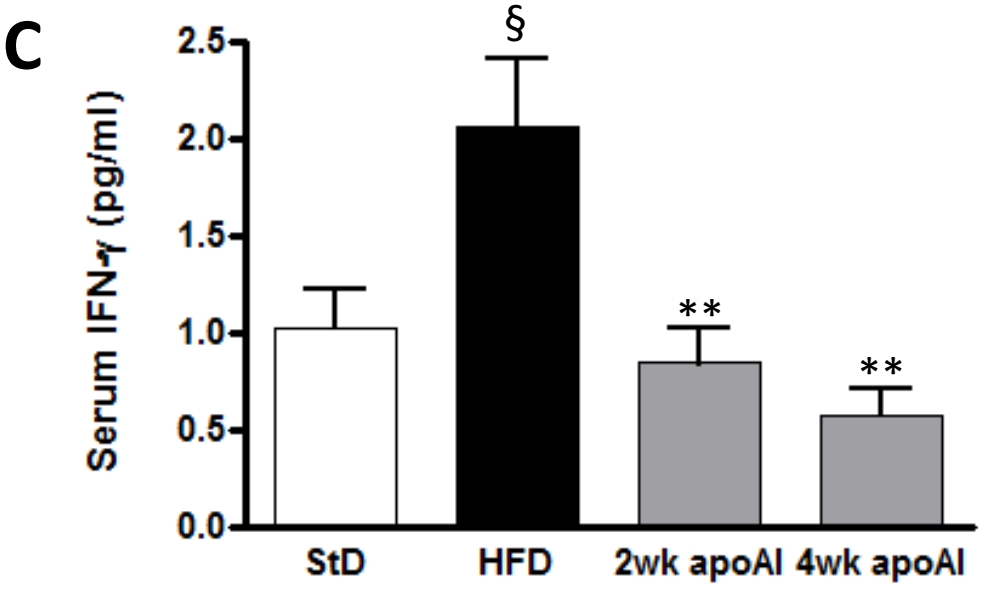
C
Serum IFN-γ (pg/ml)
2.5
2.0
1.5
1.0
0.5
0.0
§
**
**
StD
HFD
2wk apoAI
4wk apoAI

Figure 4

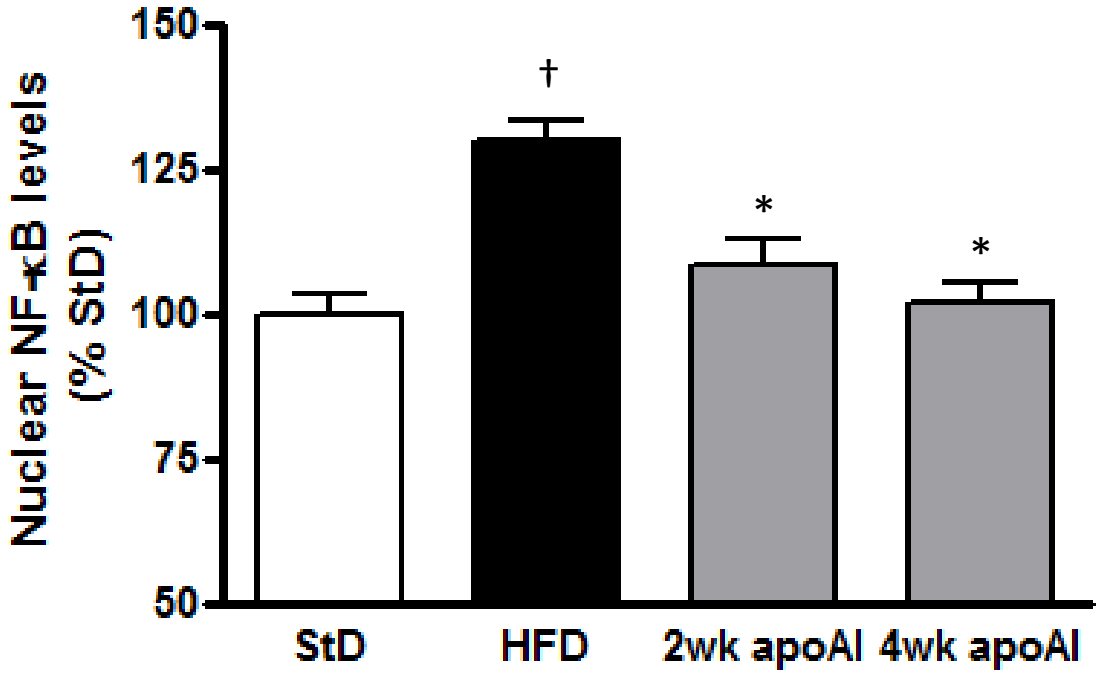
Nuclear NF-κB levels
(% StD)
150
125
100
75
50
†
*
*
StD
HFD
2wk apoAI
4wk apoAI

Figure 5

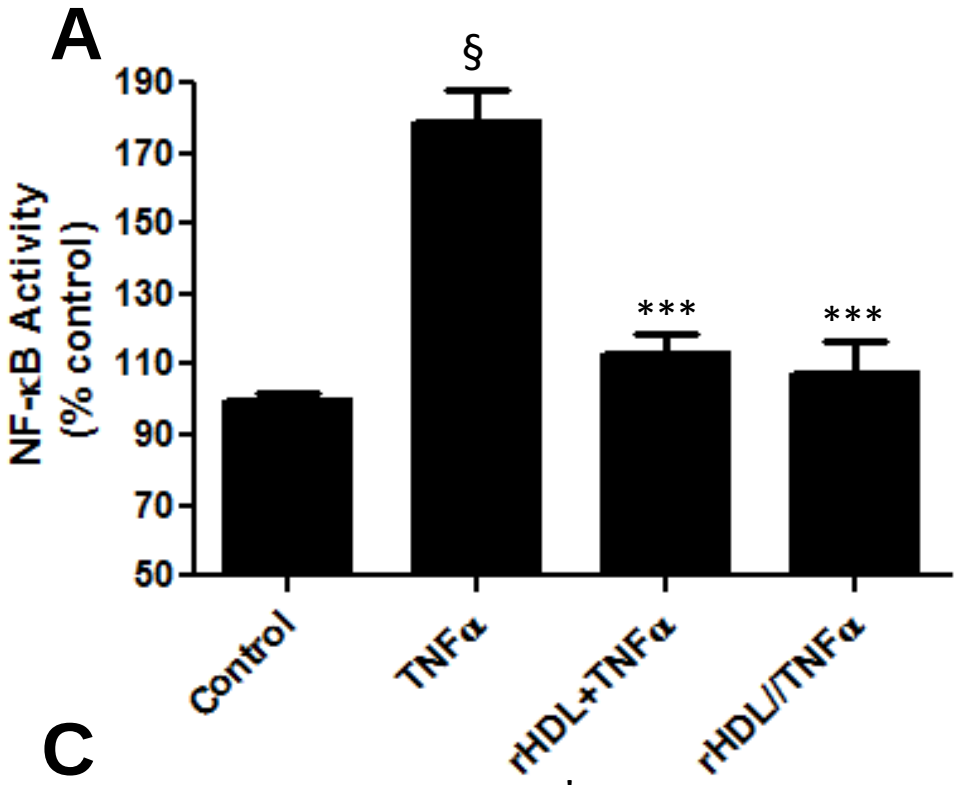
A
§
***
***
NF-κB Activity
(% control)
190
170
150
130
110
90
70
50
Control
TNFα
rHDL+TNFα
rHDL//TNFα

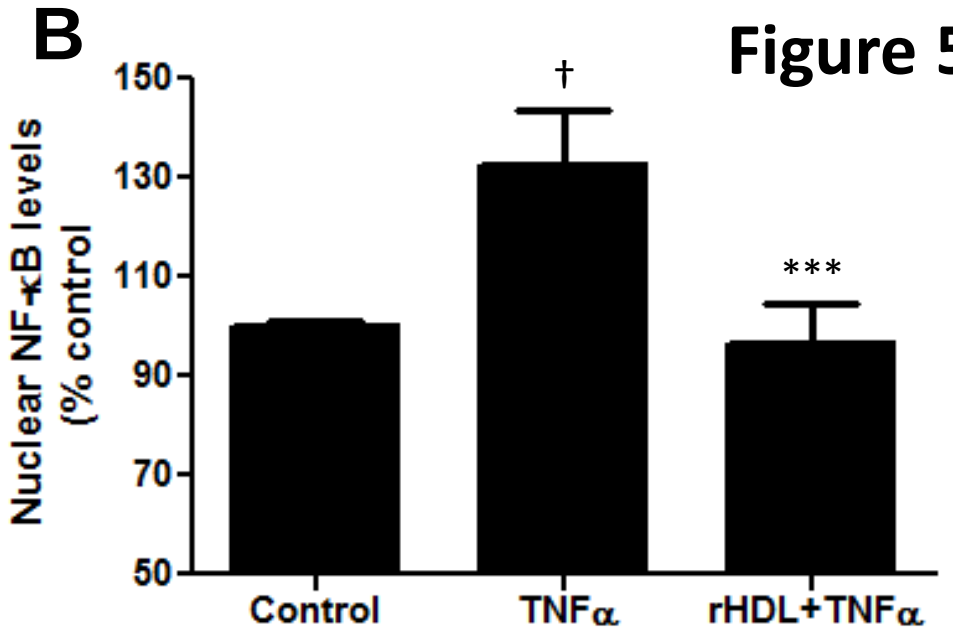
B
†
***
Nuclear NF-κB levels
(% control
150
130
110
90
70
50
Control
TNFα
rHDL+TNFα

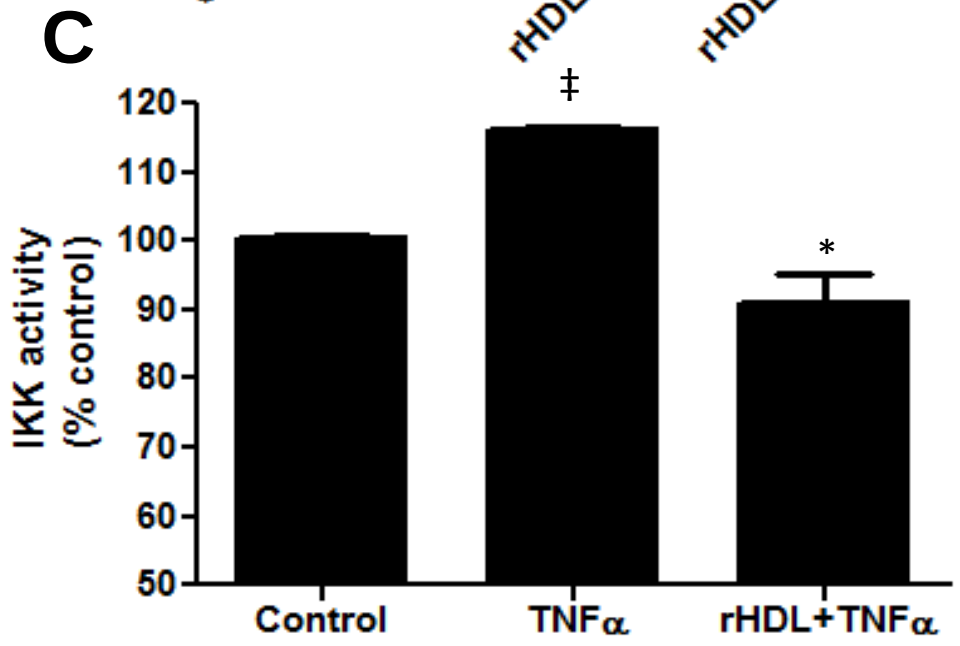
C
‡
*
IKK activity
(% control)
120
110
100
90
80
70
60
50
Control
TNFα
rHDL+TNFα

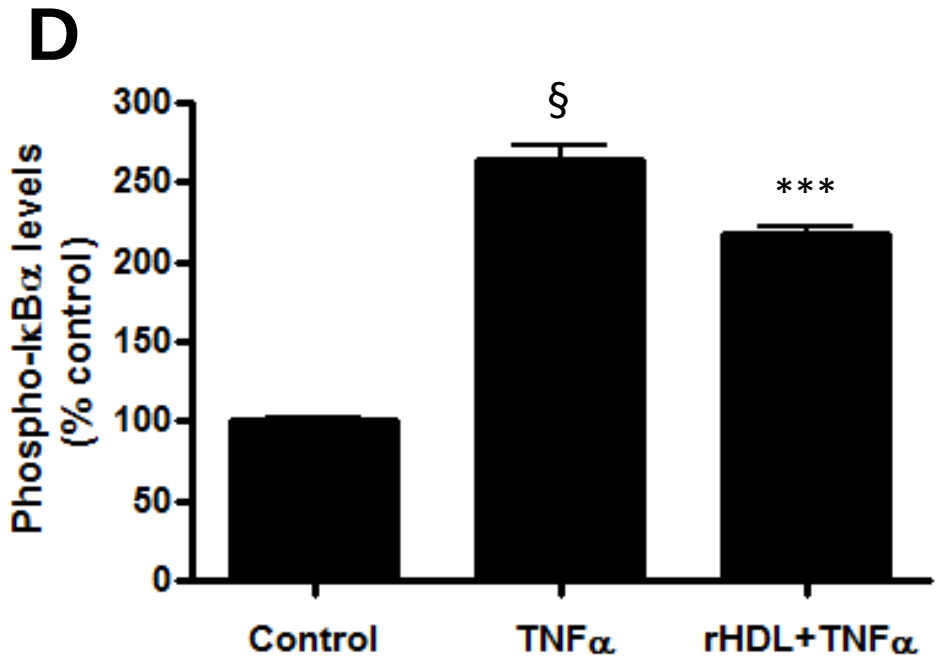
D
§
***
Phospho-IκBα levels
(% control)
300
250
200
150
100
50
0
Control
TNFα
rHDL+TNFα

Figure 6

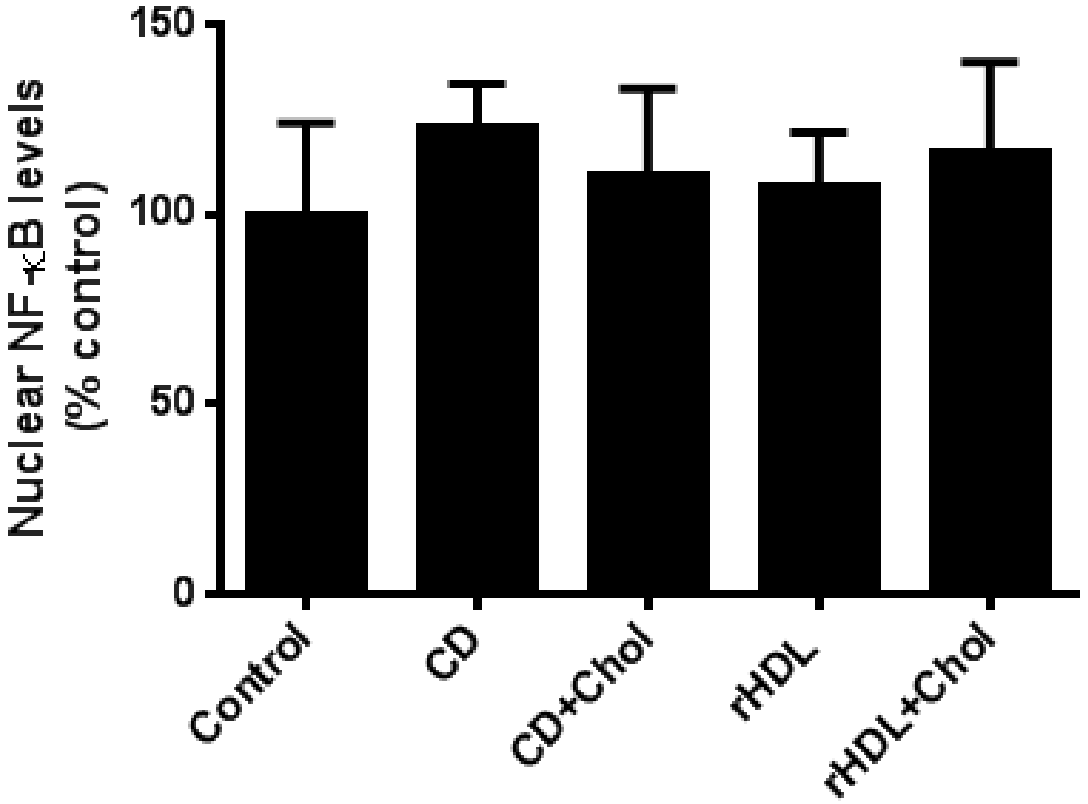
Nuclear NF-κB levels
(% control)
150
100
50
0
Control
CD
CD+Chol
rHDL
rHDL+Chol

Figure 7

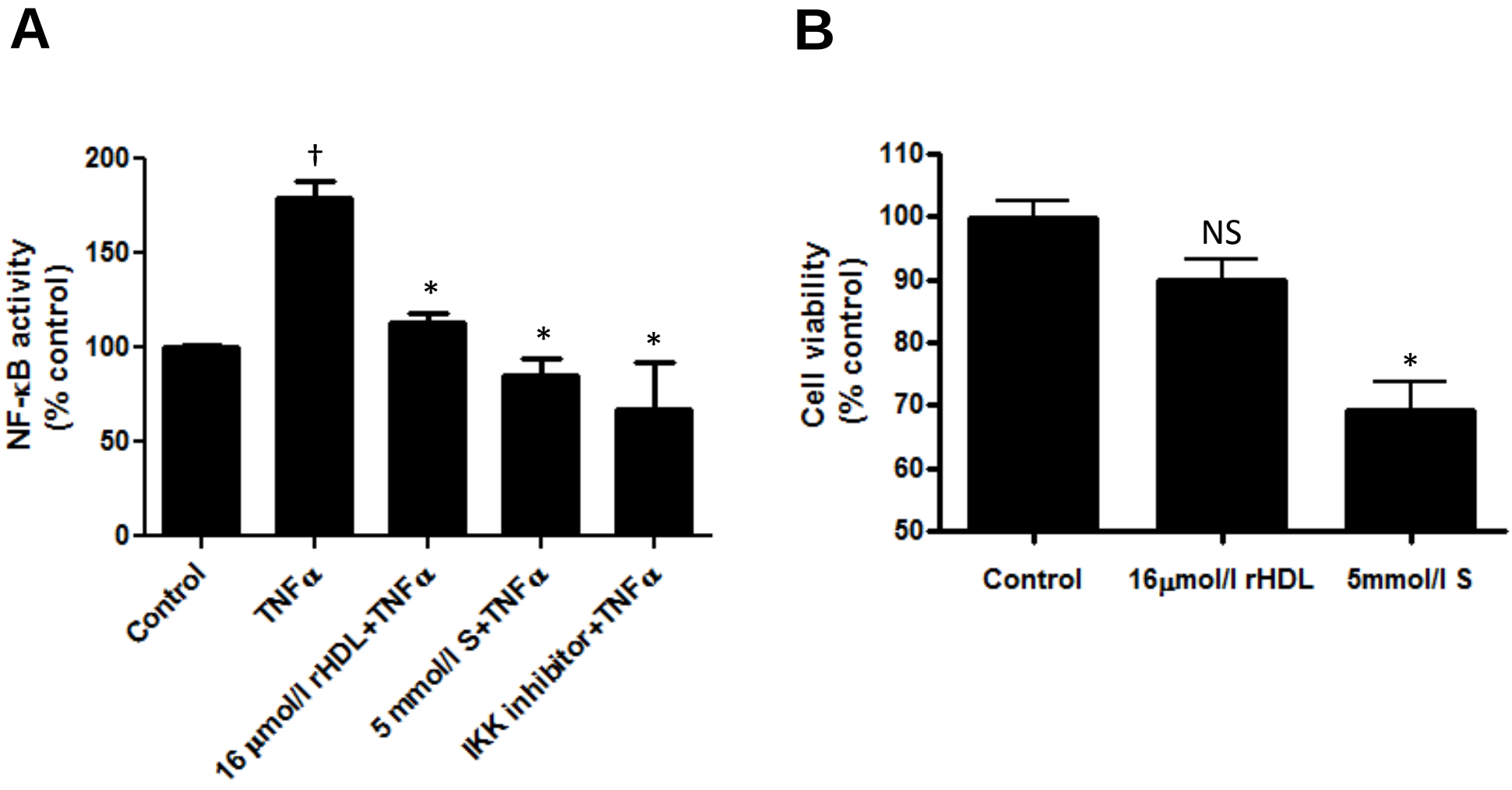
A
NF-κB activity (% control)
200
150
100
50
0
†
*
*
*
Control
TNFα
16 μmol/l rHDL+TNFα
5 mmol/l S+TNFα
IKK inhibitor+TNFα
B
Cell viability (% control)
110
100
90
80
70
60
50
NS
*
Control
16μmol/l rHDL
5mmol/l S

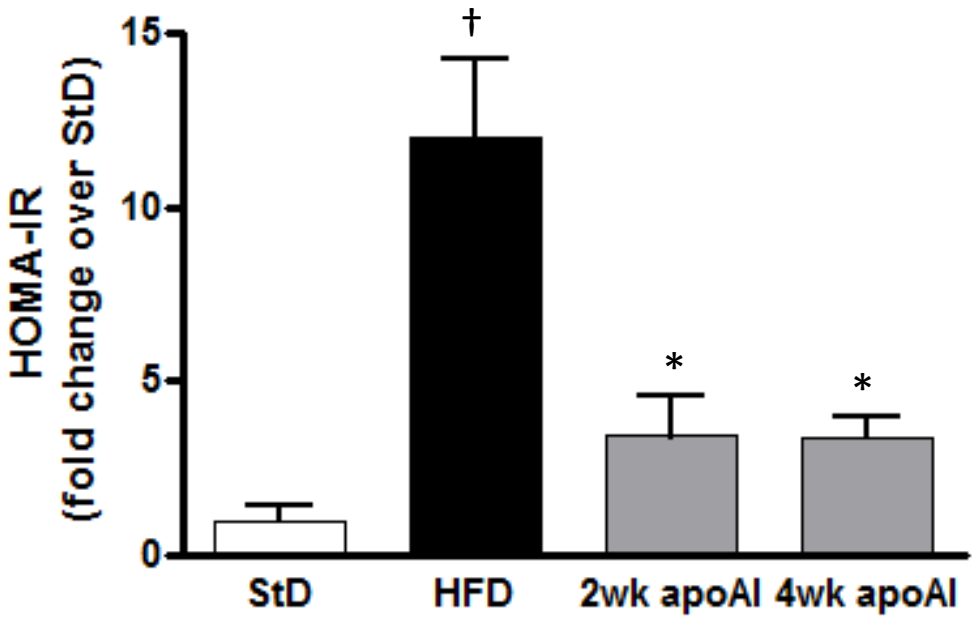
HOMA-IR
(fold change over StD)
15
10
5
0
†
*
*
StD
HFD
2wk apoAI
4wk apoAI

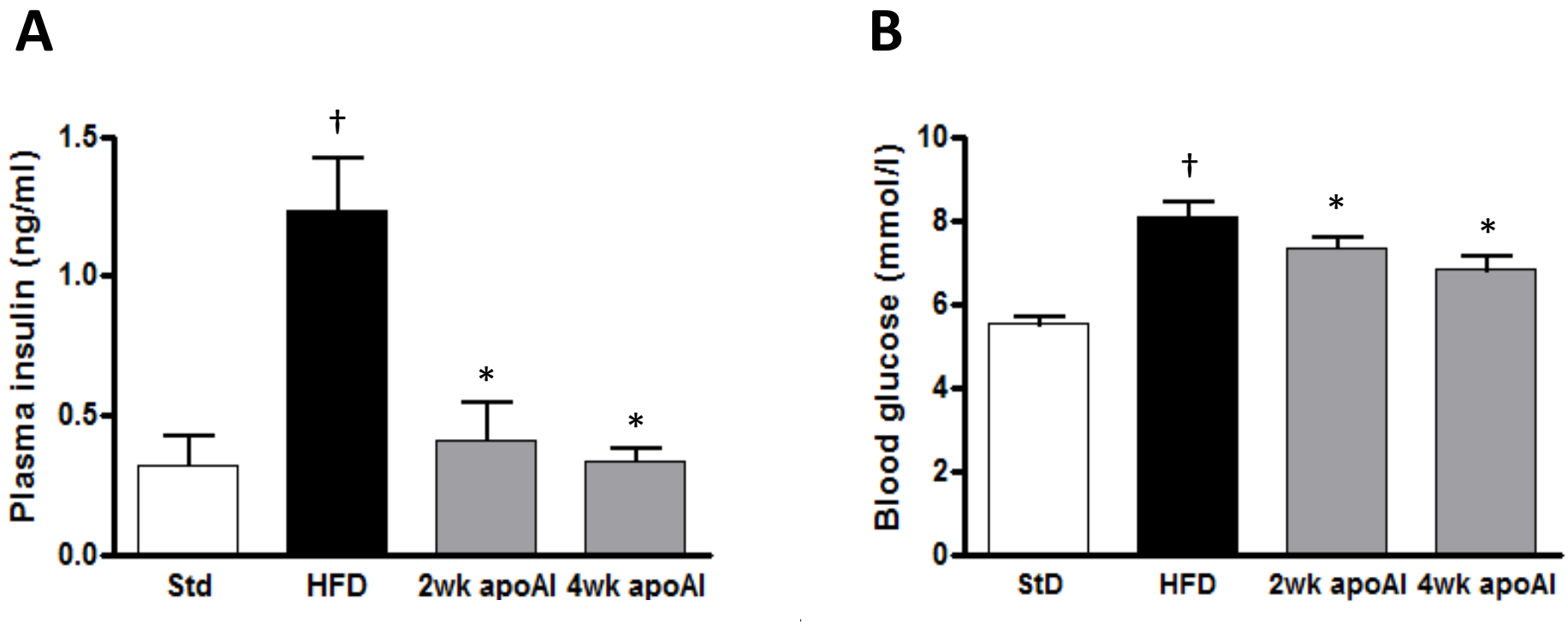
A
Plasma insulin (ng/ml)
1.5
1.0
0.5
0.0
†
*
*
Std
HFD
2wk apoAI
4wk apoAI
B
Blood glucose (mmol/l)
10
8
6
4
2
0
†
*
*
StD
HFD
2wk apoAI
4wk apoAI

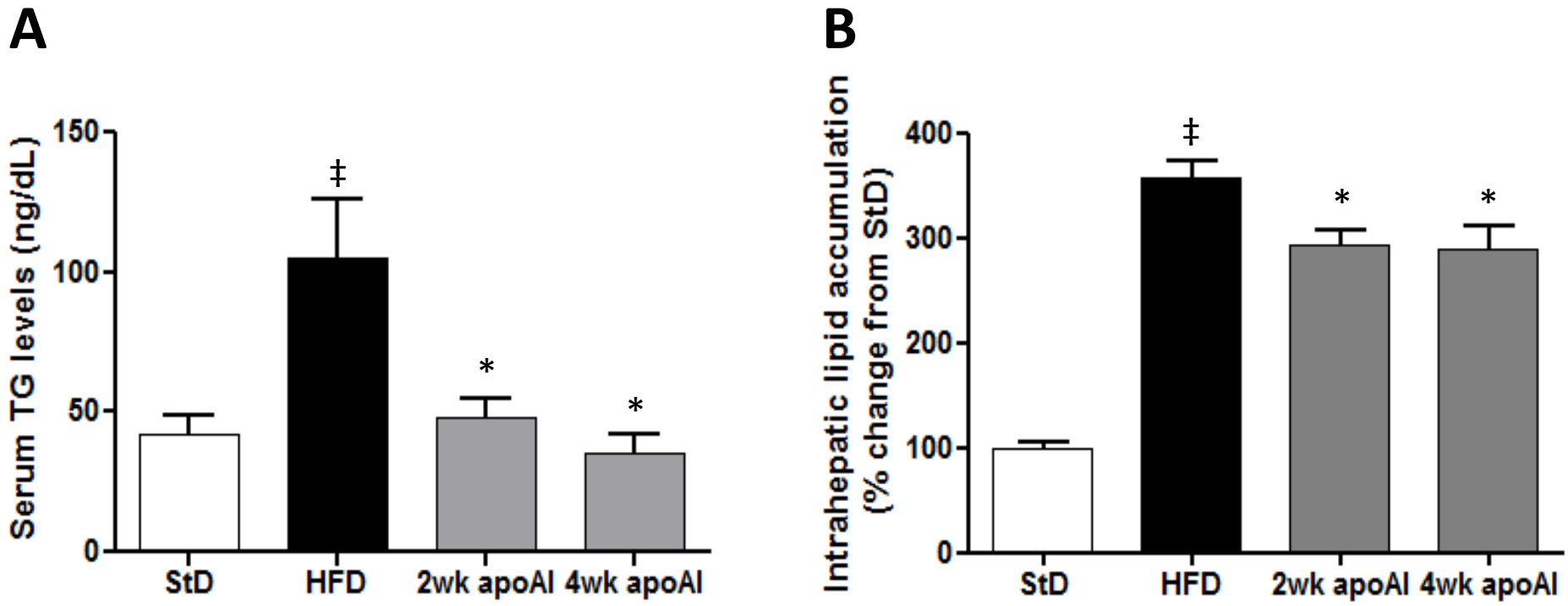
A
Serum TG levels (ng/dL)
150
100
50
0
‡
*
*
StD
HFD
2wk apoAI
4wk apoAI
B
Intrahepatic lipid accumulation
(% change from StD)
400
300
200
100
0
‡
*
*
StD
HFD
2wk apoAI
4wk apoAI

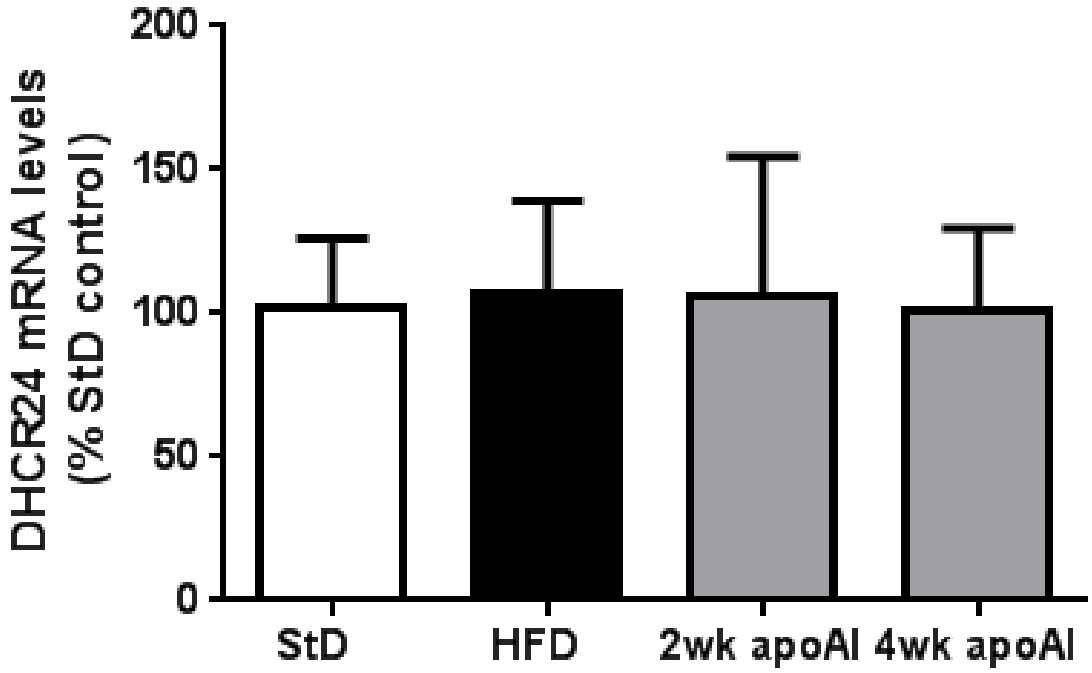
DHCR24 mRNA levels
(% StD control)
200
150
100
50
0
StD
HFD
2wk apoAI
4wk apoAI

A

PBS + TNFα

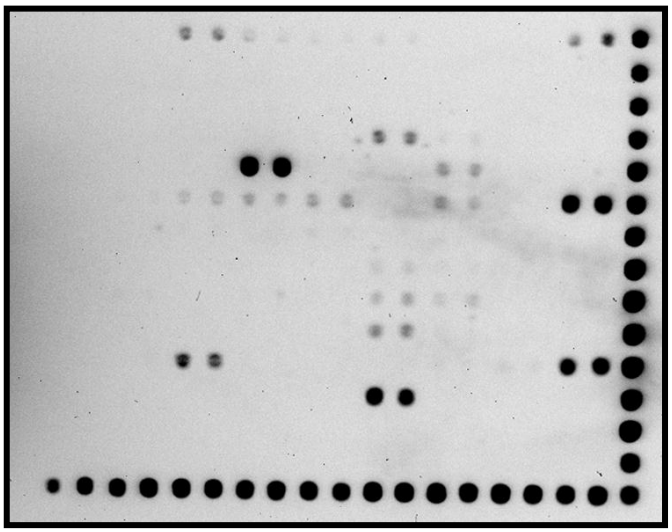

rHDL + TNFα

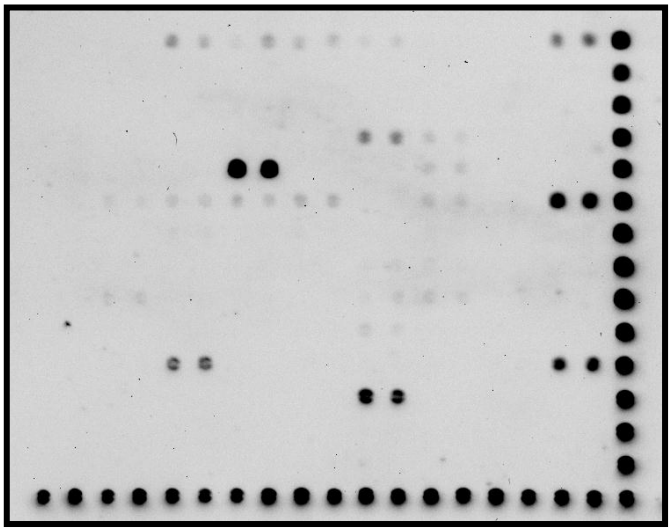

B

	1	2	3	4	5	6	7	8	9	10	11	12	13	14	15	16	17	18	
A	ALOX12	ALOX12	ADORA1	ADORA1	A1AT	A1AT	A20	A20	a1 acid GP	a1 acid GP	AGT	AGT	APOC3	APOC3	HLA-G1	HLA-G1	ACTB	ACTB	A
B	CD80	CD80	BCL-x1	BCL-x1	BCL2A1	BCL2A1	BGN	BGN	IFNb	IFNb	BDKRB1	BDKRB1	BRL1	BRL1	CCR5	CCR5			B
C	CD23	CD23	CD48	CD48	CD69	CD69	CD95	CD95	UGT8	UGT8	c-myb	c-myb	c-myc	c-myc	MMP1	MMP1			C
D	FB	FB	COX-2	COX-2	c-rel	c-rel	SCYB11	SCYB11	CYC-D1	CYC-D1	CCND3	CCND3	DDH1	DDH1	ELAM-1	ELAM-1			D
E	SCYA11	SCYA11	F8	F8	Fas-L	Fas-L	FTH	FTH	GAD65	GAD65	Gal1-R	Gal1-R	GAL-3	GAL-3	CSF3	CSF3			E
F	CSF2	CSF2	GRO1	GRO1	GSTP1	GSTP1	HMG-14	HMG-14	HMOX1	HMOX1	HAS1	HAS1	ICAM-1	ICAM-1	IFNg	IFNg	GAPDH	GAPDH	F
G	IGFBP1	IGFBP1	IGFBP-2	IGFBP-2	MAD-3	MAD-3	IL10	IL10	IL11	IL11	IL12	IL12	IL15	IL15	IL1-a	IL1-a			G
H	IL1B	IL1B	IL1RN	IL1RN	IL2	IL2	IL2-Ra	IL2-Ra	IL6	IL6	IL8	IL8	IL9	IL9	NOS	NOS			H
I	IRF1	IRF1	IRF-2	IRF-2	JUN-B	JUN-B	LAMB2	LAMB2	Lox-1	Lox-1	LYZ	LYZ	MAdCAM-1	MAdCAM-1	MCP-1	MCP-1			I
J	CSF-1	CSF-1	MDR-1	MDR-1	MIP2g	MIP2g	MMP-3	MMP-3	MMP9	MMP9	Mn-SOD	Mn-SOD	MTS1	MTS1	NPYY1	NPYY1			J
K	NFKB1	NFKB1	NFKB2	NFKB2	PRG1	PRG1	p53	p53	PAFR1	PAFR1	PAX8	PAX8	PDGF-B	PDGF-B	PTX3	PTX3	UBC	UBC	K
L	TAP1	TAP1	PENK	PENK	LMP-2	LMP-2	CD62	CD62	PTGIS	PTGIS	AGER	AGER	RANTES	RANTES	SAA	SAA			L
M	TCRB	TCRB	TNC	TNC	THBS2	THBS2	TNF	TNF	TNFb	TNFb	TNF-R	TNF-R	TGM1	TGM1	UPAR	UPAR			M
N	VCAM-1	VCAM-1	VEGFC	VEGFC	VIM	VIM	WT1	WT1	TNSFS5	TNSFS5	MSX1	MSX1	AhRR	AhRR					N
O																			O

Gene	Accession no.	Forward	Reverse
A1AT	NM_001002236	CAATGCCACCGCCATCTTCTTC	CAGTTGACCCAGGACGCTCTT
GAL3	NR_003225	CCTTCCACTTTAACCCACGCTTC	ACCGACTGTCTTTCTTCCCTTCC
GRO1	NM_001511	TGCTGCTCCTGCTCCTGGTA	GTGTGGCTATGACTTCGGTTTGG
GSTP1	NM_000852	TCGCCGCCGCAGTCTTC	GTCACCACCTCCTCCTTCCAG
IGFBP2	NM_000597	GGGAGTGCTGGTGTGTGAAC	CGGCTGGCTGCGGTCTA
1L8	NM_000584	CGGAAGGAACCATCTCACTGT	GGTCCACTCTCAATCACTCTCA
LAMB2	NM_002292	TGTGATTGTGACTCTCGTGGAAT	CAGGGATGGCAGGCAGGAA
MAD3	NM_031300	GCTGGAGGTGGATGTGGAGAG	GGCACGAGTAGAGGGCAGAG
MCP1	NM_002982	CAA TCA ATG CCC CAG TCA C	GAT TCT TGG GTT GTG GGA GTG
MNSOD	NM_001024465	CCTAACGGTGGTGGAGAAC	AACCTGAGCCTTGGACAC
TP53	NM_000546	GCATCTACAAGCAGTCACAGC	TCCACACGCAAATTTCCTTCC
PRG1	NM_003897	GCATCCTCCAGCATCTCAACTC	CTACCTCGCAGCCACCCTAAA
PTX3	NM_002852	GTGGGTGGTGGCTTTGATGAAA	GATGTGACAAGACTCTGCTCCTC
B2M	BC064910.1	CATCCAGCGTACTCCAAAGA	GACAAGTCTGAATGCTCCAC
SAA1	NM_000331	CCAATCACTTCCGACCTGCTG	GCTTTGTATCCCTGCCCTGAG
CHREBP	NM_021455.4	CTG GGG ACC TAA ACA GGA GC	GAA GCC ACC CTA TAG CTC CC
PEPCK	NM_011044.2	GGTGTTTACTGGGAAGGCATC	CAATAATGGGGCACTGGCTG
G6P	NM_008061.3	CATGGGCGCAGCAGGTGTATACT	CAAGGTAGATCCGGGACAGACAG
TNFα	BC137720.1	CTGTGAAGGGAATGGGTGTT	CTCCCTTTGCAGAACTCAGG
IL6	DQ788722.1	TGTGCAATGGCAATTCTGAT	GGAAATTGGGGTAGGAAGGA
IFNγ	BC119065.1	GAAAAGGAGTCGCTGCTGAT	CGCAATCACAGTCTTGGCTA
IL1β	M15131.1	GCTCAGGGTCACAAGAAACC	CATCAAAGCAATGTGCTGGT
CD68	BC021637.1	CCAATTCAGGGTGGAAGAAA	CTCGGGCTCTGATGTAGGTC
F4/80	X93328.1	CTCCAAGCCTATTATCTATACC	CTTCCACAATCTCACAGC
SREBP1	NM_011480.3	TTTCCTTAACGTGGGCCTAGTC	TGTCTTCGATGTCGTTCAAAACC
DHCR24	NM_053272.2	GAAGTCAACGCAAGCCTCTCC	ACATCGCCACACCCATCCC
TBP	U63933.1	GGCCTCTCAGAAGCATCACTA	GCCAAGCCCTGAGCATAA